with Alexa Fluor 488 or Alexa Fluor 594 (Invitrogen) at room temperature for 1 h. All the antibodies are listed in Table S2.

### Crystal Violet Staining

The human ESC-derived cells that had adhered to the wells were stained with 200 μl of 0.3% crystal violet solution at room temperature for 15 min. Excess crystal violet was then removed and the wells were washed three times. Fixed crystal violet was solubilized in 200 μl of 100% ethanol at room temperature for 15 min. Cell viability was estimated by measuring the absorbance at 595 nm of each well using a microtiter plate reader (Sunrise, Tecan).

### LacZ Assay

The human ESC- and iPSC-derived cells were transduced with Ad-LacZ at 3,000 VP/cell for 1.5 h. After culturing for the indicated number of days, 5-bromo-4-chloro-3-indolyl β-D-galactopyranoside (X-Gal) staining was performed as described previously [15].

## Supporting Information

**Table S1 List of Taqman probes and primers used in this study.**
(DOC)

**Table S2 List of antibodies used in this study.**
(DOC)

**Figure S1 PrE cells formation from human ESCs on day 1 of differentiation.** (A) The procedure for differentiation of human ESCs and iPSCs to ExEn cells by treatment with BMP4 (20 ng/ml) is presented schematically. (B) Human ESCs (H9) were morphologically changed during ExEn differentiation; when human ESCs were cultured with the medium containing BMP4 (20 ng/ml) for 5 days, the cells began to show flattened epithelial morphology. The scale bar represents 50 μm. (C–E) The tTemporal protein expression analysis during ExEn differentiation was performed by immunohistochemistry. The PrE markers COUP-TF1 [21] (red), SOX17 [14] (red), and SOX7 [14] (red) were detected on day 1. In contrast to the PS markers, the expression of the DE marker GSC [22] (red) was not detected and the level of the pluripotent marker NANOG (green) declined between day 0 and day 1. Nuclei were counterstained with DAPI (blue). The scale bar represents 50 μm.
(PDF)

**Figure S2 Mesendoderm cells formation from human ESCs on day 3 of differentiation.** (A) The procedure for differentiation of human ESCs and iPSCs to DE cells by treatment with Activin A (100 ng/ml) is presented schematically. hESF-GRO medium was supplemented with 5 factors and 0.5 mg/ml fatty acid free BSA, as described in the Materials and Methods. (B) Human ESCs (H9) were morphologically changed during DE differentiation; when human ESCs were cultured with the medium containing Activin A (100 ng/ml) for 5 days, the morphology of the cells began to show visible cell-cell boundaries. The scale bar represents 50 μm. (C–E) The tTemporal protein expression analysis during DE differentiation was performed by immunohistochemistry. The anterior PS markers FOXA2 [21] (red), GSC [22] (red), and SOX17 [14] (red) were adequately detected on day 3. The PS marker T [45] (red) was detected until day 3. In contrast to the PS markers, the expression of the pluripotent marker NANOG [24] (green) declined between day 2 and day 3. Nuclei were counterstained with DAPI (blue). The scale bar represents 50 μm.
(PDF)

**Figure S3 Overexpression of SOX17 mRNA in human ESC (H9)-derived PS cells by Ad-SOX17 transduction.** Human ESC-derived PS cells (day 1) were transduced with 3,000VP/cell of Ad-SOX17 for 1.5 h. On day 3 of differentiation, real-time RT-PCR analysis of the SOX17 expression was performed in Ad-LacZ-transduced cells and Ad-SOX17-transduced cells. On the y axis, the expression levels of undifferentiated human ESCs on day 0 was were taken defined as 1.0. All data are represented as the means±SD ($n = 3$).
(PDF)

**Figure S4 Efficient transduction in Activin A-induced human ESC (H9)-derived cells by using a fiber-modified Ad vector containing the EF-1α promoter.** Undifferentiated human ESCs and Activin A-induced human ESC-derived cells, which were cultured with the medium containing Activin A (100 ng/ml) for 0, 1, 2, 3, and 4 days, were transduced with 3,000 vector particles (VP)/cell of Ad-LacZ for 1.5 h. The day after transduction, X-gal staining was performed. The scale bar represents 100 μm. Similar results were obtained in two independent experiments.
(PDF)

**Figure S5 Optimization of the time period for Ad-SOX17 transduction to promote DE differentiation from human iPSCs (Tic).** Undifferentiated human iPSCs and Activin A-induced human iPSC-derived cells, which were cultured with the medium containing Activin A (100 ng/ml) for 0, 1, 2, 3, and 4 days, were transduced with 3,000 VP/cell of Ad-SOX17 for 1.5 h. Ad-SOX17-transduced cells were cultured with Activin A (100 ng/ml) until day 5, and then real-time RT-PCR analysis was performed. The horizontal axis represents the day on which the cells were transduced with Ad-SOX17. On the y axis, the expression levels of undifferentiated cells on day 0 was were taken defined as 1.0. All data are represented as the means±SD ($n = 3$).
(PDF)

**Figure S6 Time course of LacZ expression in human ESC (H9)-derived mesendoderm cells transduced with Ad-LacZ.** The hHuman ESC-derived mesendoderm cells (day 3) were transduced with 3,000 VP/cell of Ad-LacZ for 1.5 h. On days 4, 5, 6, 8, and 10, X-gal staining was performed. Note that human ESC-derived cells were passaged on day 5. The scale bar represents 100 μm. Similar results were obtained in two independent experiments.
(PDF)

**Figure S7 Optimization of the time period for Ad-SOX17 transduction into Activin A-induced human ESC (H9)-derived cells.** Undifferentiated human ESCs and Activin A-induced hESC-derived cells, which were cultured with the medium containing Activin A (100 ng/ml) for 0, 1, 2, 3, and 4 days, were transduced with 3,000 VP/cell of Ad-LacZ or Ad-SOX17 for 1.5 h. Ad-SOX17-transduced cells were cultured with Activin A (100 ng/ml) until day 5, then the cell viability was evaluated with crystal violet staining. The horizontal axis represents the day on which the cells were transduced with Ad-SOX17. On the y axis, the level of non-transduced cells was taken defined as 1.0. All data are represented as the means±SD (n = 3).
(PDF)

**Figure S8 Model of differentiation of human ESCs and iPSCs into ExEn and DE cells by stage-specific SOX17 transduction.** The ExEn and DE differentiation process is divided into at least two stages. In the first stage, human ESCs differentiate into either PrE cells by treatment with BMP4 (20 ng/ml) or mesendoderm cells by treatment with Activin A (100 ng/

ml). In the second stage, SOX17 promotes the further differentiation of each precursor cell into ExEn and DE cells, respectively. We have demonstrated that the efficient differentiation of these two distinct endoderm lineages is accomplished by stage-specific SOX17 transduction.
(PDF)

## Acknowledgments

We thank Hiroko Matsumura and Misae Nishijima for their excellent technical support. We thank Mr. David Bennett and Ms. Ong Tyng Tyng for critical reading of the manuscript.

## Author Contributions

Conceived and designed the experiments: K. Takayama MI K. Kawabata MFK HM. Performed the experiments: K. Takayama MI K. Tashiro. Analyzed the data: K. Takayama MI K. Kawabata K. Tashiro K. Katayama FS HM. Contributed reagents/materials/analysis tools: K. Kawabata K. Katayama FS TH MFK HM. Wrote the paper: K. Takayama K. Kawabata HM.

## References

1. Enders AC, Given RL, Schlafke S (1978) Differentiation and migration of endoderm in the rat and mouse at implantation. Anat Rec 190: 65–77.
2. Gardner RL (1983) Origin and differentiation of extraembryonic tissues in the mouse. Int Rev Exp Pathol 24: 63–133.
3. Grapin-Botton A, Constam D (2007) Evolution of the mechanisms and molecular control of endoderm formation. Mech Dev 124: 253–278.
4. Tam PP, Kanai-Azuma M, Kanai Y (2003) Early endoderm development in vertebrates: lineage differentiation and morphogenetic function. Curr Opin Genet Dev 13: 393–400.
5. Thomson JA, Itskovitz-Eldor J, Shapiro SS, Waknitz MA, Swiergiel JJ, et al. (1998) Embryonic stem cell lines derived from human blastocysts. Science 282: 1145–1147.
6. Takahashi K, Tanabe K, Ohnuki M, Narita M, Ichisaka T, et al. (2007) Induction of pluripotent stem cells from adult human fibroblasts by defined factors. Cell 131: 861–872.
7. Yu J, Vodyanik MA, Smuga-Otto K, Antosiewicz-Bourget J, Frane JL, et al. (2007) Induced pluripotent stem cell lines derived from human somatic cells. Science 318: 1917–1920.
8. Xu RH, Chen X, Li DS, Li R, Addicks GC, et al. (2002) BMP4 initiates human embryonic stem cell differentiation to trophoblast. Nat Biotechnol 20: 1261–1264.
9. Pera MF, Andrade J, Houssami S, Reubinoff B, Trounson A, et al. (2004) Regulation of human embryonic stem cell differentiation by BMP-2 and its antagonist noggin. J Cell Sci 117: 1269–1280.
10. Seguin CA, Draper JS, Nagy A, Rossant J (2008) Establishment of endoderm progenitors by SOX transcription factor expression in human embryonic stem cells. Cell Stem Cell 3: 182–195.
11. Gouon-Evans V, Boussemart L, Gadue P, Nierhoff D, Koehler CI, et al. (2006) BMP-4 is required for hepatic specification of mouse embryonic stem cell-derived definitive endoderm. Nat Biotechnol 24: 1402–1411.
12. Niakan KK, Ji H, Maehr R, Vokes SA, Rodolfa KT, et al. (2010) Sox17 promotes differentiation in mouse embryonic stem cells by directly regulating extraembryonic gene expression and indirectly antagonizing self-renewal. Genes Dev 24: 312–326.
13. Inamura M, Kawabata K, Takayama K, Tashiro K, Sakurai F, et al. (2011) Efficient Generation of Hepatoblasts From Human ES Cells and iPS Cells by Transient Overexpression of Homeobox Gene HEX. Mol Ther 19: 400–407.
14. Kanai-Azuma M, Kanai Y, Gad JM, Tajima Y, Taya C, et al. (2002) Depletion of definitive gut endoderm in Sox17-null mutant mice. Development 129: 2367–2379.
15. Kawabata K, Sakurai F, Yamaguchi T, Hayakawa T, Mizuguchi H (2005) Efficient gene transfer into mouse embryonic stem cells with adenovirus vectors. Mol Ther 12: 547–554.
16. Koizumi N, Mizuguchi H, Utoguchi N, Watanabe Y, Hayakawa T (2003) Generation of fiber-modified adenovirus vectors containing heterologous peptides in both the HI loop and C terminus of the fiber knob. J Gene Med 5: 267–276.
17. Fujikura J, Yamato E, Yonemura S, Hosoda K, Masui S, et al. (2002) Differentiation of embryonic stem cells is induced by GATA factors. Genes Dev 16: 784–789.
18. Koutsourakis M, Langeveld A, Patient R, Beddington R, Grosveld F (1999) The transcription factor GATA6 is essential for early extraembryonic development. Development 126: 723–732.
19. Morrisey EE, Tang Z, Sigrist K, Lu MM, Jiang F, et al. (1998) GATA6 regulates HNF4 and is required for differentiation of visceral endoderm in the mouse embryo. Genes Dev 12: 3579–3590.
20. Kunath T, Strumpf D, Rossant J (2004) Early trophoblast determination and stem cell maintenance in the mouse--a review. Placenta 25 Suppl A: S32–38.
21. Sasaki H, Hogan BL (1993) Differential expression of multiple fork head related genes during gastrulation and axial pattern formation in the mouse embryo. Development 118: 47–59.
22. Blum M, Gaunt SJ, Cho KW, Steinbeisser H, Blumberg B, et al. (1992) Gastrulation in the mouse: the role of the homeobox gene goosecoid. Cell 69: 1097–1106.
23. Morrison GM, Oikonomopoulou I, Migueles RP, Soneji S, Livigni A, et al. (2008) Anterior definitive endoderm from ESCs reveals a role for FGF signaling. Cell Stem Cell 3: 402–415.
24. Mitsui K, Tokuzawa Y, Itoh H, Segawa K, Murakami M, et al. (2003) The homeoprotein Nanog is required for maintenance of pluripotency in mouse epiblast and ES cells. Cell 113: 631–642.
25. Shalaby F, Rossant J, Yamaguchi TP, Gertsenstein M, Wu XF, et al. (1995) Failure of blood-island formation and vasculogenesis in Flk-1-deficient mice. Nature 376: 62–66.
26. D'Amour KA, Agulnick AD, Eliazer S, Kelly OG, Kroon E, et al. (2005) Efficient differentiation of human embryonic stem cells to definitive endoderm. Nat Biotechnol 23: 1534–1541.
27. Shiojiri N (1984) The origin of intrahepatic bile duct cells in the mouse. J Embryol Exp Morphol 79: 25–39.
28. Ingelman-Sundberg M, Oscarson M, McLellan RA (1999) Polymorphic human cytochrome P450 enzymes: an opportunity for individualized drug treatment. Trends Pharmacol Sci 20: 342–349.
29. Murry CE, Keller G (2008) Differentiation of embryonic stem cells to clinically relevant populations: lessons from embryonic development. Cell 132: 661–680.
30. Qu XB, Pan J, Zhang C, Huang SY (2008) Sox17 facilitates the differentiation of mouse embryonic stem cells into primitive and definitive endoderm in vitro. Dev Growth Differ 50: 585–593.
31. Sherwood RI, Jitianu C, Cleaver O, Shaywitz DA, Lamenzo JO, et al. (2007) Prospective isolation and global gene expression analysis of definitive and visceral endoderm. Dev Biol 304: 541–555.
32. Shimoda M, Kanai-Azuma M, Hara K, Miyazaki S, Kanai Y, et al. (2007) Sox17 plays a substantial role in late-stage differentiation of the extraembryonic endoderm in vitro. J Cell Sci 120: 3859–3869.
33. Yasunaga M, Tada S, Torikai-Nishikawa S, Nakano Y, Okada M, et al. (2005) Induction and monitoring of definitive and visceral endoderm differentiation of mouse ES cells. Nat Biotechnol 23: 1542–1550.
34. Gadue P, Huber TL, Paddison PJ, Keller GM (2006) Wnt and TGF-beta signaling are required for the induction of an in vitro model of primitive streak formation using embryonic stem cells. Proc Natl Acad Sci U S A 103: 16806–16811.
35. Levinson-Dushnik M, Benvenisty N (1997) Involvement of hepatocyte nuclear factor 3 in endoderm differentiation of embryonic stem cells. Mol Cell Biol 17: 3817–3822.
36. Spence JR, Lange AW, Lin SC, Kaestner KH, Lowy AM, et al. (2009) Sox17 regulates organ lineage segregation of ventral foregut progenitor cells. Dev Cell 17: 62–74.
37. Mizuguchi H, Hayakawa T (2004) Targeted adenovirus vectors. Hum Gene Ther 15: 1034–1044.
38. Furue MK, Na J, Jackson JP, Okamoto T, Jones M, et al. (2008) Heparin promotes the growth of human embryonic stem cells in a defined serum-free medium. Proc Natl Acad Sci U S A 105: 13409–13414.
39. Makino H, Toyoda M, Matsumoto K, Saito H, Nishino K, et al. (2009) Mesenchymal to embryonic incomplete transition of human cells by chimeric OCT4/3 (POU5F1) with physiological co-activator EWS. Exp Cell Res 315: 2727–2740.
40. Nagata S, Toyoda M, Yamaguchi S, Hirano K, Makino H, et al. (2009) Efficient reprogramming of human and mouse primary extra-embryonic cells to pluripotent stem cells. Genes Cells 14: 1395–1404.
41. Mizuguchi H, Kay MA (1998) Efficient construction of a recombinant adenovirus vector by an improved in vitro ligation method. Hum Gene Ther 9: 2577–2583.
42. Mizuguchi H, Kay MA (1999) A simple method for constructing E1- and E1/E4-deleted recombinant adenoviral vectors. Hum Gene Ther 10: 2013–2017.
43. Tashiro K, Kawabata K, Sakurai H, Kurachi S, Sakurai F, et al. (2008) Efficient adenovirus vector-mediated PPAR gamma gene transfer into mouse embryoid bodies promotes adipocyte differentiation. J Gene Med 10: 498–507.
44. Maizel JV, Jr., White DO, Scharff MD (1968) The polypeptides of adenovirus. I. Evidence for multiple protein components in the virion and a comparison of types 2, 7A, and 12. Virology 36: 115–125.
45. Wilkinson DG, Bhatt S, Herrmann BG (1990) Expression pattern of the mouse T gene and its role in mesoderm formation. Nature 343: 657–659.

Research Article

Biomedical Chromatography

Received 16 April 2010, Revised 3 June 2010, Accepted 4 June 2010 Published online in Wiley Online Library: 27 July 2010

(wileyonlinelibrary.com) DOI 10.1002/bmc.1486

# Determination of sulfate ester content in sulfated oligo- and poly-saccharides by capillary electrophoresis with indirect UV detection

**Mitsuhiro Kinoshita[a], Naotaka Kakoi[a], Yu-ki Matsuno[b], Takao Hayakawa[c] and Kazuaki Kakehi[a]***

**ABSTRACT: Carbohydrates having sulfate groups such as glycosaminoglycans and chemically synthesized sucrose sulfate show interesting and important biological activities. We adapted CE with indirect UV detection technique to the determination of sulfate ester in sulfated carbohydrates, which were previously hydrolyzed with HCl. The liberated sulfate ion was analyzed using a background electrolyte consisting of triethanolamine-buffered chromate with hexamethonium bromide. Sulfate contents of glucose 3-sulfate and sucrose octasulfate used as a model were in good agreement with theoretical values (accuracy, 95.9–96.7 and 97.4–101.9%, respectively), and relative standard deviation values run-to-run were 0.977 and 1.90%, respectively. We applied the method to the determination of the sulfate contents of some glycosaminoglycan samples and showed that the contents were in good agreement with those calculated from sulfur content. Copyright © 2010 John Wiley & Sons, Ltd.**

**Keywords**: sulfate; glycosaminoglycans; capillary electrophoresis indirect UV detection

## Introduction

Sulfation of hydroxyl and amino groups (-O-$SO_3H$ and -NH-$SO_3H$) is one of the common modifications of carbohydrates and is often observed in various glycoconjugates such as proteoglycans or mucin-like glycoproteins. Sulfated carbohydrates are widely distributed in animals as the major constituents of proteoglycans and are biologically active molecules involved in various biological events (Hooper *et al.*, 1996; Honke and Taniguchi, 2002; Wu, 2006). Functions of sulfated carbohydrates strongly depend on the presence and spatial positioning in the molecules. Degree of sulfation on carbohydrates is also closely related to biological activities such as blood coagulation, signal transduction and cell–cell interaction (Lindahl *et al.*, 1983; Villanueva, 1984; Hemmerich and Rosen, 1994; Small *et al.*, 1996; Tsuboi *et al.*, 1996). Chemical sulfation of carbohydrates often affords compounds showing novel biological activities such as anti-HIV activities (Katsuraya *et al.*, 1994, 1999; Yoshida *et al.*, 1995; Hattori *et al.*, 1998). Sulfated carbohydrates also have potential as pharmaceuticals (Werz and Seeberger, 2005). Sucrose octasulfate, 'Sucralfate' and the chemically synthesized octasulfated pentasaccharide 'Arixtra' are used as antiulcer and anticoagulant drugs, respectively (Candelli *et al.*, 2000; Giangrande, 2002).

In view of these interesting features of sulfated carbohydrates, assessment of sulfate content is important not only for the understanding of their biological significance but also the development and manufacturing of novel bioactive sulfated carbohydrates. Several methods have been developed for the determination of sulfate content of carbohydrates. Classical methods are based on the colorimetric determination of the inorganic sulfate ion liberated from sulfated carbohydrates by acid hydrolysis, such as chelating barium ions with rhodizonate (Terho and Hartiala, 1971; Roy and Turner, 1982). Srinivasan *et al.* achieved the determination of microgram quantity of sulfate ion based on the formation of stable complex of sulfate ester with *n*-butylamine and achieved determination of microgram quantity of sulfate ion (Srinivasan *et al.*, 1970). Unfortunately, these methods are not suitable for the determination of a small amount of sulfate ester in complex carbohydrate, because they are time-consuming and not sensitive enough, require a significant amount of material, and are prone to interference from the other ions. Compared with these conventional methods, ion chromatography (IC) demonstrates increased specificity and sensitivity

* Correspondence to: K. Kakehi, Faculty of Pharmaceutical Sciences, Kinki University, Kowakae 3-4-1, Higashi-osaka 577-8502, Japan. E-mail: k_kakehi@phar.kindai.ac.jp

[a] Faculty of Pharmaceutical Sciences, Kinki University, Kowakae 3-4-1, Higashi-osaka 577-8502, Japan

[b] Research Center for Medical Glycoscience, National Institute of Advanced Industrial Science and Technology, Open Space Laboratory C-2, 1-1-1 Umezono, Tsukuba, Ibaraki 305-8568, Japan

[c] Pharmaceutical Research and Technology Institute, Kinki University, Kowakae 3-4-1, Higashi-osaka 577-8502, Japan

**Abbreviations used:** BGE, background electrolyte; CSA, chondroitin sulfate A; DMF, *N,N*-dimethylformamide; DS, dermatan sulfate; GAG, glycosaminoglycan; HA, hyaluronic acid; HMB, hexamethonium bromide; HP, heparin; HS, heparan sulfate; TBA, tributylamine; TEA, triethanolamine.

as well as the inherent ability for the determination of various inorganic ions, and has been applied to the analysis of the ions in the samples from biological, environmental and industrial origins (Lopez-Ruiz, 2000). The sulfate contents in glycoproteins or GAGs were successfully determined by IC (Cole and Evrovski, 1997; Toida *et al.*, 1999). Toida *et al.* liberated the sulfate ion from chemically O-sulfated GAGs by acid hydrolysis, and determined it by a combination of IC and conductivity detection (Tadano-Aritomi *et al.*, 2001).

Capillary electrophoresis (CE) is a powerful tool for separation of inorganic ions with high resolving power. Its performance is comparable with that of IC, and has become one of the standard tools for the analysis of inorganic ions in environmental, biomedical, clinical and industrial samples (Fritz, 2000; Timerbaev, 2002, 2004; Johns *et al.*, 2003; Pacakova *et al.*, 2003; Paull and King, 2003). CE allows rapid analysis with high resolution and exhibits good capabilities in quantitative analysis, making it well suited for routine analysis of sulfate content of carbohydrates. Although the detection in CE is usually performed by direct UV detection, most inorganic ions lack a chromophore and cannot be detected using common direct UV detection. Therefore, indirect UV detection technique is usually used for determination of inorganic ions. Indirect UV detection adds an UV-absorbing co-ion (called the probe) to the background electrolyte (BGE) and this probe is displaced by migration, causing a negative signal. Indirect UV detection is an effective alternative detection technique for inorganic ions. The attractive performance of the CE method has been employed for the assay of sulfotransferase activity (Saillard *et al.*, 1999). Thus, CE is considered a useful alternative to the well-established IC method for routine analysis of sulfate content of carbohydrates.

In the present study, we developed a method using capillary electrophoresis with indirect UV detection to the determination of sulfate content of sulfated oligo-/polysaccharides, and applied the method for the determination of sulfate content in some sulfated GAGs and the monitoring of chemically sulfation reaction of polysaccharides. The present method will provide a robust method for the analysis of sulfated carbohydrates using routinely available laboratory instrumentation.

## Experimental

### Materials

Hexamethonium bromide, glucose 3-sulfate (sodium salt, 98% purity by HPLC), sucrose octasulfate (sodium salt) and heparin from bovine intestinal mucosa were purchased from Sigma (St Louis, MO, USA). Hyaluronic acid (from *Streptococcus zooepidemicus*) was purchased from Nacalai tesque (Uji, Kyoto, Japan). Chondroitin sulfate A (from whale cartilage), dermatan sulfate (from pig skin) and heparan sulfate (from bovine kidney) were purchased from Seikagaku Biobusiness (Chiyoda-ku, Tokyo, Japan). Tributylamine (TBA), *N,N*-dimethylformamide (DMF) and pyridine–sulfur trioxide complex were obtained from Wako Pure Chemicals (Dosho-machi, Osaka, Japan). All other chemicals and reagents were of the highest grade or HPLC grade. Running buffers and aqueous solutions were prepared with water purified with a Milli-Q purification system (Millipore, Bedford, MS, USA).

### Sulfation of Chondroitin Sulfate A

Chemical sulfation of chondroitin sulfate A was performed according to the method reported by Maruyama *et al.* (1998). The sodium salt (10 mg) of chondroitin sulfate A (from whale cartilage) was dissolved in 1 mL of 5% TBA–HCl water (pH 2.8), and then the solution was lyophilized to dryness to give the tributylammonium salt. The salt was dissolved in 1 mL of DMF, and pyridine–sulfur trioxide complex (10, 50, 100 and 250 mg) was added. After incubating the mixture for 1 h at 40°C, the reaction was terminated by addition of water (1 mL). The reaction product was precipitated with cold ethanol (6 mL) saturated with anhydrous sodium acetate, collected by centrifugation at 4°C, then dissolved in water followed by dialysis against water to remove salts and lyophilized. We obtained $PSCS_{10}$ (11.8 mg), $PSCS_{50}$ (14.1 mg), $PSCS_{100}$ (17.2 mg) and $PSCS_{250}$ (18.6 mg), respectively, by changing the amount of pyridine–sulfur trioxide complex.

### Sample and Standard Solutions

Standard solutions of sulfate ion were prepared by dissolving an accurately weighed amount of sodium sulfate (300 mg) in water (10 mL; 210 mM). A series of standard solutions of sulfate ion for calibration curve were prepared by appropriate dilution of the standard solution with water. Sample solution of sulfated oligo-/polysaccharides was also prepared by dissolving an accurately weighed amount (1.00 mg) in of water (1 mL).

### CE Analysis of Sulfate Ion with Indirect UV Detection

CE was performed with a Beckman P/ACE MDQ system equipped with a UV detector (Beckman Coulter, Fullerton, CA, USA). A fused silica capillary (50 μm i.d., 56 cm effective length, 66 cm total length, from Agilent Technologies) was used throughout the work. The background electrolyte was composed of 10 mM $CrO_3$–2 mM hexamethonium bromide in 10% MeOH–water (pH 8.0) adjusted with triethanolamine. The background electrolyte was passed through a cellulose acetate membrane filter (0.2 μm). Prior to the first run, the capillary was rinsed with 0.1 M NaOH for 10 min, followed by washing with water for 10 min, and then filled with the background electrolyte. The capillary was conditioned by pre-electrophoresis (–20 kV) for 10 min. After washing the capillary with water and filling with the background electrolyte, samples were automatically injected using pressure injection mode at 1.0 psi for 10 s. Electrophoresis was performed at –20 kV using reverse polarity. Detection was carried out with monitoring the UV absorption at 254 nm. The negative peaks due to the presence of anions in the background of $CrO_3$ were automatically converted into positive peaks by Beckman 32 Karat software version 4.0 (Beckman Coulter).

### Hydrolysis of Sulfated Carbohydrates

A standard solution (20 μL) of glucose 3-sulfate was mixed with 20 μL of 1 M HCl and the mixture was kept at 100°C in a polypropylene tube for specified times. After cooling the mixture to room temperature, the solution (40 μL) was diluted with 1000 μL of water. An aqueous solutions (1000 μL) of $NaNO_3$ was added to the mixture as internal standard and an aliquot (20 μL) was used for the analysis of sulfate ion.

### Standard Procedure for the Determination of Sulfate Content in Sulfated Oligo- and Polysaccharides

A solution (20 μL) of sodium salt of sulfated oligo- or polysaccharides was mixed with 20 μL of 1 M HCl, and the mixture was kept at 100°C for 2 h. After cooling the mixture to room temperature, water and the internal standard solutions were added to the mixture as described above and an aliquot was used for the determination of sulfate ion. The content of sulfate ion was calculated from the calibration curve obtained from standard solutions of $Na_2SO_4$. The percentages of sulfate content were calculated using the following equation:

$$SO_3\,(w/w) = (\text{wt of } SO_4^{2-} \times (\text{wt of } SO_3/\text{wt of } SO_4)/\text{wt of sample}) \times 100$$

where wt (weight) of $SO_3$ = 80, wt of $SO_4^{2-}$ = 96, wt of $SO_4^{2-}$ (μg) in hydrolysates is the amount calculated using the calibration curve, and wt of the sample is the amount of the sample in micrograms.

## Results and Discussion

### Principle

The method is based on the acid hydrolysis of sulfonic acid ester (-O-$SO_3H$ and -NH-$SO_3H$) followed by the determination of the released sulfate ion ($SO_4^{2-}$) with CE with indirect UV detection technique. Sulfated oligo-/polysaccharides are hydrolyzed with HCl to produce $SO_4^{2-}$. In CE, indirect detection is conveniently available for the detection of compounds which do not have chromophores/fluorophores. When non-UV absorbing sulfate ion passes through the UV detector, the zone of $SO_4^{2-}$ causes a negative signal in the background electrolyte containing a UV-absorbing compound as probe. The output polarity of the detection is reversed so that a positive peak is obtained. The content of sulfate ester in parent compounds is calculated using the calibration curve obtained from a standard solution of $Na_2SO_4$.

### Selection of the Background Electrolyte

Selection of the electrolyte (e.g. co-ion and electroosmotic modifier) is important for the sensitive and quantitative determination of sulfate ion. In the present study, chromate ion was selected as the UV absorbing co-ion (probe ion) because of its ionic mobility being close to that of $SO_4^{2-}$, which ensures high peak symmetry (Johns *et al.*, 2003; Pacakova *et al.*, 2003). We had to pay attention on the presence of high excess amount of chloride ion ($Cl^-$) in the sample solutions due to the HCl employed for the hydrolysis of sulfate-containing carbohydrates. Inorganic anions by CE are usually analyzed under negative polarity using electroosmotic modifiers such as cationic surfactant, polymer and amines, which improve resolutions of the ions (Haddad *et al.*, 1999; Harakuwe *et al.*, 1999; Kaniansky *et al.*, 1999). Muzikar *et al.* (2003) reported the determination of trace amount of inorganic anions (e.g. $SO_4^{2-}$ or $NO_3^-$) in the presence of large excess of $Cl^-$ using an electrolyte consisting of triethanolamine (TEA)-buffered chromate with hexamethonium bromide (HMB) as electroosmotic modifier. In the present study, $SO_4^{2-}$ (0.21 mM as $Na_2SO_4$) was successfully analyzed in the presence of 50 mM HCl using this condition, and $Cl^-$ and $SO_4^{2-}$ were completely resolved and observed at 4.50 and 4.85 min, respectively (Fig. 1a).

We employed nitrate ion ($NO_3^-$) as internal standard (50 μg/mL, 0.59 mM; Fig. 1b). Ions of $SO_4^{2-}$ and $NO_3^-$ with a huge amount of $Cl^-$ were completely resolved within 5 min. Based on these results, 10 mM $CrO_3$–2 mM HMB in 10% MeOH–water (pH 8.0 adjusted with TEA) was selected as the background electrolyte throughout the present study.

### Linearity and Limit of Detection

The calibration curve for absolute peak area of sulfate ion showed good linearity between 5.0 and 625 μg/mL ($y = 65.4x + 0.58$, $R = 0.9996$; Fig. 2a). In the case of correction of the injection amount by internal standard, the calibration curve exhibited excellent linearity ($y = 0.015x + 0.22$, $R = 0.9999$; Fig. 2b). Both lower limit of detection (LOD) and lower limit of quantification (LOQ) were evaluated on the basis of the standard deviation ($\sigma$) and slope ($S$) from the calibration curve of $SO_4^{2-}$. In the present conditions, LOD ($= 3\sigma/S$) and LOQ ($= 10\sigma/S$) were 0.934 and 3.113 μg/mL, respectively.

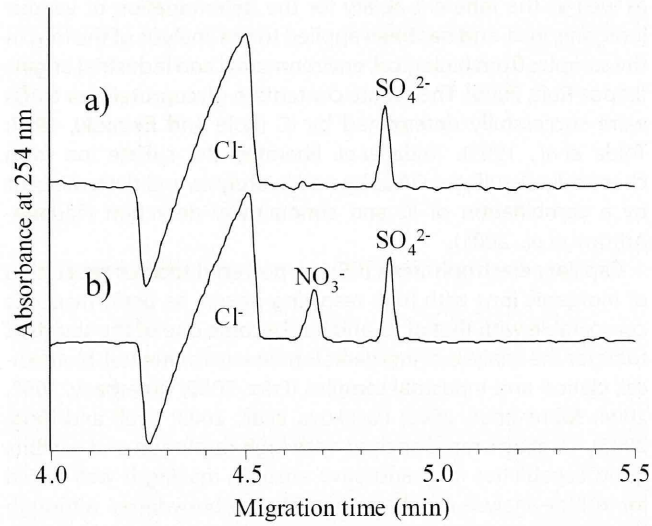


**Figure 1.** Separation of inorganic anions by CE with indirect UV detection: (a) 0.21 mM sulfate and 50 mM chloride; (b) 0.21 mM sulfate, 50 mM chloride, and 0.59 mM nitrate. Background electrolyte: 10 mM $CrO_3$/2 mM hexamethonium bromide in 10% MeOH–water at pH 8.0 adjusted with triethanolamine. Capillary: a fused silica capillary (i.d., 50 μm; effective length 56 cm). Applied voltage, –20 kV; temperature, 25°C; sample injection, hydrodynamic injection (1.0 psi, 10 s); detection, indirect UV absorption at 254 nm.

### Reproducibility

Run-to-run reproducibility of migration times of $SO_4^{2-}$ and $NO_3^-$ was evaluated using a mixture of 30 μg/mL $Na_2SO_4$ and 50 μg/mL $NaNO_3$. Migration times of $SO_4^{2-}$ and $NO_3^-$ were 4.96 ± 0.08 and 4.68 ± 0.07, respectively. The relative standard deviation (RSD) was less than 1.4 and 1.6%, respectively ($n = 5$).

### Precision

We obtained RSD values in absolute determination of $SO_4^{2-}$ using standard solutions of $Na_2SO_4$ at 5, 30 and 312.5 μg/mL. The RSD (%) of $SO_4^{2-}$ peak area were 4.58, 2.24 and 2.83%, respectively ($n = 5$; Table 1). In contrast, when using the internal standard ($NO_3^-$), the RSD (%) of $SO_4^{2-}$ was 1.84, 0.69 and 1.69%, respectively ($n = 5$; Table 1).

### Optimization of Conditions for Liberation of $SO_4^{2-}$ by Acid Hydrolysis

Conditions for liberation of $SO_4^{2-}$ from sulfated carbohydrates by acid hydrolysis with HCl were optimized using glucose 3-sulfate as model. After hydrolysis of glucose 3-sulfate with 1 M HCl at 100°C for specified intervals, a portion of the reaction mixture was diluted with water. An aqueous solution of the internal standard ($NaNO_3$) was added, and the released $SO_4^{2-}$ was determined according to the conditions described above.

The content of $SO_4^{2-}$ in the reaction mixture was dependent on hydrolysis time and the hydrolysis was completed within 2 h as shown in Fig. 3(a, b). The excess chloride ion and free glucose produced by hydrolysis in the mixture did not show interference in the determination of $SO_4^{2-}$. The amount of sulfate ion in glucose 3-sulfate was estimated as 28.1 w/w% (0.96 mol/mol), and showed good agreement with the theoretical values (28.4%). Recoveries were 95.9–96.7% ($n = 5$).

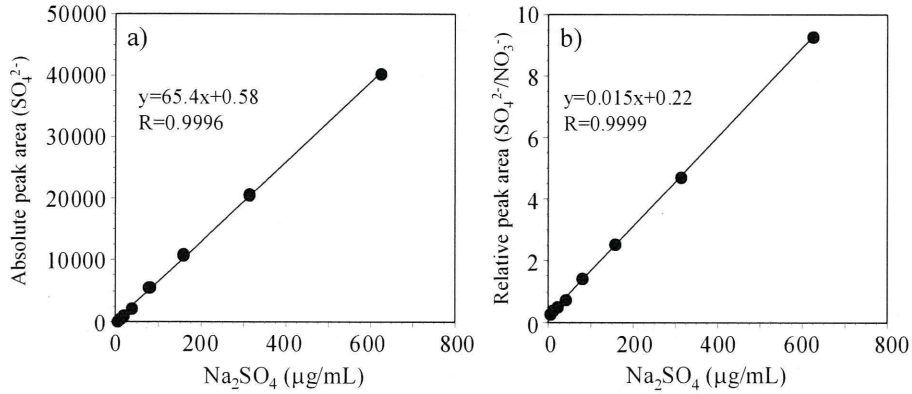


**Figure 2.** Calibration curve for determination of sulfate ions. (a) Concentration of $Na_2SO_4$ vs absolute peak area of $SO_4^{2-}$. (b) Concentration of $Na_2SO_4$ vs relative peak area ($SO_4^{2-}/NO_3^-$).

**Table 1.** Precision results of determination of sulfate ion at three different concentrations

| Run | Peak area | | | | | | | | |
|---|---|---|---|---|---|---|---|---|---|
| | 5 μg/mL $Na_2SO_4$ | | | 30 μg/mL $Na_2SO_4$ | | | 312.5 μg/mL $Na_2SO_4$ | | |
| | $SO_4^{2-}$ | $NO_3^-$ | $SO_4^{2-}/NO_3^-$ | $SO_4^{2-}$ | $NO_3^-$ | $SO_4^{2-}/NO_3^-$ | $SO_4^{2-}$ | $NO_3^-$ | $SO_4^{2-}/NO_3^-$ |
| 1 | 462 | 361 | 1.280 | 2755 | 2043 | 1.349 | 28041 | 21505 | 1.304 |
| 2 | 492 | 378 | 1.302 | 2647 | 1957 | 1.353 | 29945 | 22869 | 1.309 |
| 3 | 506 | 402 | 1.259 | 2798 | 2092 | 1.337 | 28762 | 22214 | 1.295 |
| 4 | 476 | 362 | 1.315 | 2695 | 1989 | 1.355 | 27945 | 22290 | 1.254 |
| 5 | 518 | 409 | 1.267 | 2679 | 2008 | 1.334 | 29013 | 22452 | 1.292 |
| Average | 491 | 382 | 1.284 | 2715 | 2018 | 1.346 | 28741 | 22266 | 1.291 |
| SD | 22.5 | 22.3 | 0.024 | 60.8 | 51.9 | 0.009 | 813.6 | 495.1 | 0.022 |
| RSD% | 4.58 | 5.83 | 1.838 | 2.24 | 2.57 | 0.687 | 2.83 | 2.22 | 1.694 |

We evaluated linearity, repeatability, precision and lower limit of detection using sucrose octasulfate. Sucrose octasulfate is a cytoprotective drug widely used to prevent or treat several gastrointestinal diseases such as gastro-esophageal reflux, gastritis, peptic ulcer, stress ulcer and dyspepsia (Lam and Ching, 1994; Candelli *et al.*, 2000). The sulfate content found in the hydrolysate of sucrose octasulfate showed a good linear relationship with sucrose octasulfate (0.03–1 mg/mL). The value for the relative standard deviation ($n = 5$) of determination of sucrose octasulfate was 1.90% at 250 μg/mL. The limit of detection was 7.8 μg/mL as a solution of sucrose octasulfate sodium salt. When a solution (250 μg/mL) of sucrose octasulfate sodium salt was used, the sulfate content of one batch was 53.1% (accuracy 97.4–101.9%, $n = 5$), which is very close to the theoretical value (54.2%).

### Determination of Sulfate Content in Various GAG Samples

Glycosaminoglycans (GAGs) are a family of highly complex and polydisperse linear polysaccharides that display a variety of important biological roles (Jackson *et al.*, 1991; Scott, 1992; Bourin and Lindahl, 1993; Sugahara and Kitagawa, 2000). GAGs are categorized into some main structural groups: hyaluronic acid (HA), chondroitin sulfate A (CSA), dermatan sulfate (DS), heparin (HP) and heparan sulfate (HS) (Zaia, 2009). The structural complexity is compounded by their sequence heterogeneity, primarily caused by variation of the degree and position of sulfate groups. We applied the present method to the determination of sulfate content in some GAG samples. The results are shown in Fig. 4 and Table 2.

Among five GAG samples used in the study, CSA, DS, HP and HS showed sulfate contents of 14.2, 15.0, 25.1 and 11.5%, respectively. HP is mainly composed of trisulfated disaccharide units, α(1-4)-linked L-iduronic acid, which is 2-*O*-sulfated, and D-glucosamine, which is *N*- and 6-*O*-sulfated (Zaia, 2009). Therefore, the sulfate content of HP is higher than those of CSA and DS, which are sulfated at only 4-OH of GalNAc in the disaccharide unit. The sulfate content of HS is lower than those of other sulfated GAGs, because HS from bovine kidney contains unsulfated repeating disaccharide units (GlcAβ1–4GlcNAc) as the major component (~60%), and contains the monosulfated GlcA β1–4GlcNAc (~25%) and the di- or tri-sulfated IdoAα1–4GlcNAc (~15%) (Zaia, 2009). HA, composed of non-sulfated disaccharide units, does not contain sulfate. When hydrolysis step was not included, we did not observe sulfate ions in the electropherograms for all these GAG samples (data not shown). This indicates that inorganic sulfate ion was negligible in the sample. The sulfate contents found in five GAGs were in good agreement with those calculated from sulfur contents provided by the manufacturer (Table 2).

### Application to the Monitoring of Chemical Sulfation of Chondroitin Sulfate

Chemical modification of polysaccharides such as sulfation affords novel biological activity, and has been well studied (Srinivasan *et al.*, 1970; Suzuki *et al.*, 2001). We synthesized some preparations of sulfated chondroitin sulfate having different degree of sulfation by changing the amount of pyridine–sulfur

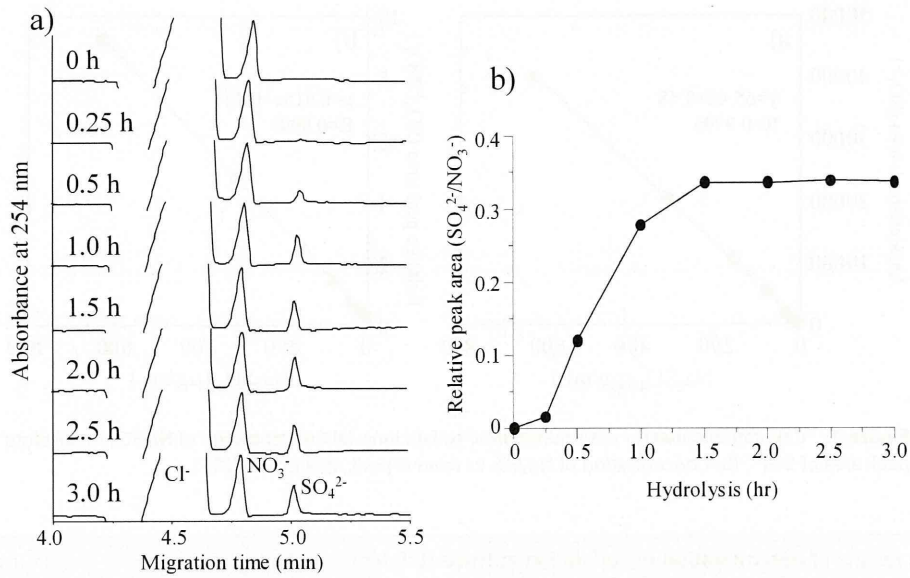


**Figure 3.** Time course of sulfate liberation during hydrolysis of the glucose 3-sulfate with HCl. (a) Electropherograms of the reaction mixture after hydrolysis. (b) Time course of liberation of sulfate ion from glucose 3-sulfate.

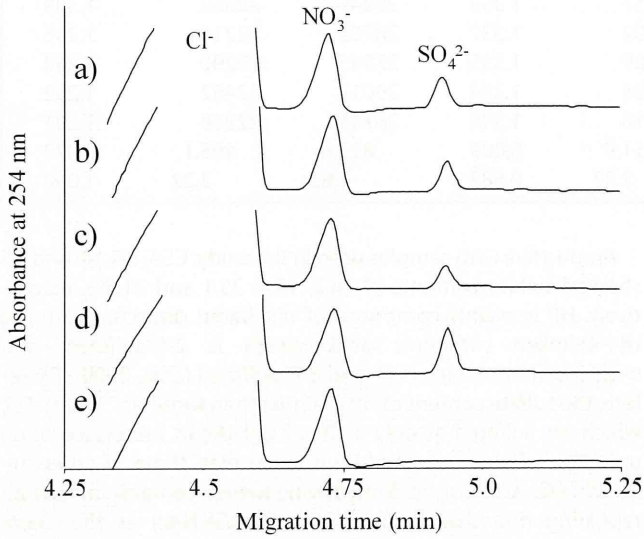


**Figure 4.** Determination of the sulfate content of some glycosaminoglycans. (a) Chondroitin sulfate A; (b) dermatan sulfate; (c) heparan sulfate; (d) heparin; and (e) hyaluronic acid.

trioxide complex according to the method reported by Maruyama *et al.* (1998). The $PSCS_{10}$, $PSCS_{50}$, $PSCS_{100}$ and $PSCS_{250}$ were obtained from 10 mg CS using 10, 50, 100, and 250 mg pyridine–sulfur complex, respectively. Each preparation was analyzed by the present technique (Table 3).

Sulfate contents calculated from the preparations of $PSCS_{10}$, $PSCS_{50}$, $PSCS_{100}$ and $PSCS_{250}$ were 24.7, 38.5, 45.5 and 48.09%, respectively. The results showed that the amount of pyridine–surfur trioxide complex used in the reaction caused remarkable differences in the sulfate contents, and showed that the present method is useful for monitoring the degree of sulfation during chemical sulfation of oligo-/polysaccharides.

**Table 2.** Sulfate contents of GAGs

| GAGs | Total sulfate (%)[a] | |
|---|---|---|
| | Present method | Schoniger method[b] |
| Hyaluronic acid | n.d.[c] | <0.5 |
| Chondroitin sulfate A | 14.2 ± 0.5 | 15.0 |
| Dermatan sulfate | 15.0 ± 0.5 | 15.5 |
| Heparin | 25.1 ± 0.5 | 25.6 |
| Heparan sulfate | 11.5 ± 0.5 | 11.3 |

[a] Calculated from the dry weight of GAGs.
[b] Total sulfate contents were calculated from sufur contents provided by manufacturer.
[c] Not detected.

## Conclusion

In the present study, we developed a simple, robust and reliable method for the determination of sulfate content in sulfated carbohydrates using CE with indirect UV detection. The background electrolyte consisting of TEA-buffered chromate with HMB is the most appropriate for the analysis of sulfate ion liberated from parent compounds after hydrolysis with HCl.

We applied the present method to the determination of sulfate content in some sulfated GAG samples such as chondroitin sulfate, dermatan sulfate, heparin and heparan sulfate. The sulfate contents found in these GAGs were in good agreement with those obtained by conventional methods. We also applied the method to the determination of sulfate content in chemically sulfated chondroitin sulfate, and revealed the degree of sulfation.

Easy operation of the proposed technique is useful for the determination of sulfate content of sulfated oligo-/polysaccharides. The present method is suitable for routine analysis of sulfate content of carbohydrates.

**Table 3.** Sulfate contents of chemically sulfated chondroitin sulfate

| Sample | Amount of pyridine–sufur trioxide complex | Total sulfate content (%) | Degree of sulfation (%)[b] |
|---|---|---|---|
| CSA[a] | — | 14.2 | 27.5 |
| $PSCS_{10}$ | 10 mg | 24.7 | 47.6 |
| $PSCS_{50}$ | 50 mg | 38.5 | 74.6 |
| $PSCS_{100}$ | 100 mg | 45.5 | 88.2 |
| $PSCS_{250}$ | 250 mg | 48.1 | 93.2 |

[a] Chondroitin sulfate A from whale cartilage.
[b] Relative percentage to theoretical value (51.6%) of fully sulfated CSA-30mer.

## References


Bourin MC and Lindahl U. Glycosaminoglycans and the regulation of blood coagulation. *Biochemistry Journal* 1993; **289**(Pt 2): 313–330.

Candelli M, Carloni E, Armuzzi A, Cammarota G, Ojetti V, Pignataro G, Santoliquido A, Pola R, Pola E, Gasbarrini G and Gasbarrini A. Role of sucralfate in gastrointestinal diseases. *Panminerva Medicine* 2000; **42**(1): 55–59.

Cole DE, Evrovski J. Quantitation of sulfate and thiosulfate in clinical samples by ion chromatography. *Journal of Chromatography A* 1997; **789**(1–2): 221–232.

Fritz JS. Recent developments in the separation of inorganic and small organic ions by capillary electrophoresis. *Journal of Chromatography A* 2000; **884**(1–2): 261–275.

Giangrande PL. Fondaparinux (Arixtra): a new anticoagulant. *International Journal of Clinical Practice* 2002; **56**(8): 615–617.

Haddad PR, Doble P and Macka M. Developments in sample preparation and separation techniques for the determination of inorganic ions by ion chromatography and capillary electrophoresis. *Journal of Chromatography A* 1999; **856**(1–2): 145–177.

Harakuwe AH, Haddad PR and Davies NW. Effect of drying on the degradation of cationic surfactants and separation performance in capillary zone electrophoresis of inorganic anions. *Journal of Chromatography A* 1999; **863**(1): 81–87.

Hattori K, Yoshida T, Nakashima H, Premanathan M, Aragaki R, Mimura T, Kaneko Y, Yamamoto N and Uryu T. Synthesis of sulfonated aminopolysaccharides having anti-HIV and blood anticoagulant activities. *Carbohydrate Research* 1998; **312**(1–2): 1–8.

Hemmerich S and Rosen SD. 6′-sulfated sialyl Lewis x is a major capping group of GlyCAM-1. *Biochemistry* 1994; **33**(16): 4830–4835.

Honke K and Taniguchi N. Sulfotransferases and sulfated oligosaccharides. *Medical Research Review* 2002; **22**(6): 637–654.

Hooper LV, Manzella SM and Baenziger JU. From legumes to leukocytes: biological roles for sulfated carbohydrates. *FASEB Journal* 1996; **10**(10): 1137–1146.

Jackson RL, Busch SJ and Cardin AD. Glycosaminoglycans: molecular properties, protein interactions, and role in physiological processes. *Physiology Review* 1991; **71**(2): 481–539.

Johns C, Macka M and Haddad PR. Enhancement of detection sensitivity for indirect photometric detection of anions and cations in capillary electrophoresis. *Electrophoresis* 2003; **24**(12–13): 2150–2167.

Kaniansky D, Masar M, Marak J and Bodor R. Capillary electrophoresis of inorganic anions. *Journal of Chromatography A* 1999; **834**(1–2): 133–178.

Katsuraya K, Ikushima N, Takahashi N, Shoji T, Nakashima H, Yamamoto N, Yoshida T and Uryu, T. Synthesis of sulfated alkyl malto- and laminara-oligosaccharides with potent inhibitory effects on AIDS virus infection. *Carbohydrate Research* 1994; **260**(1): 51–61.

Katsuraya K, Nakashima H, Yamamoto N and Uryu T. Synthesis of sulfated oligosaccharide glycosides having high anti-HIV activity and the relationship between activity and chemical structure. *Carbohydrate Research* 1999; **315**(3–4): 234–242.

Lam SK and Ching CK. Sucralfate in clinical practice. *Journal of Gastroenterology and Hepatology* 1994; **9**(4): 401–411.

Lindahl U, Backstrom G and Thunberg L. The antithrombin-binding sequence in heparin. Identification of an essential 6-O-sulfate group. *Journal of Biological Chemistry* 1983; **258**(16): 9826–9830.

Lopez-Ruiz B. Advances in the determination of inorganic anions by ion chromatography. *Journal of Chromatography A* 2000; **881**(1–2): 607–627.

Maruyama T, Toida T, Imanari T, Yu G and Linhardt RJ. Conformational changes and anticoagulant activity of chondroitin sulfate following its O-sulfonation. *Carbohydrate Research* 1998; **306**(1–2): 35–43.

Muzikar M, Havel J and Macka M. Capillary electrophoresis determinations of trace concentrations of inorganic ions in large excess of chloride: soft modelling using artificial neural networks for optimisation of electrolyte composition. *Electrophoresis* 2003; **24**(12–13): 2252–2258.

Pacakova V, Coufal P, Stulik K and Gas B. The importance of capillary electrophoresis, capillary electrochromatography, and ion chromatography in separations of inorganic ions. *Electrophoresis* 2003; **24**(12–13): 1883–1891.

Paull B and King M. Quantitative capillary zone electrophoresis of inorganic anions. *Electrophoresis* 2003; **24**(12–13): 1892–1934.

Roy AB and Turner J. The sulphatase of ox liver. XXIV. The glycosulphatase activity of sulphatase a. *Biochimica Biophysica Acta* 1982; **704**(2): 366–373.

Saillard S, Gareil P, Jozefonvicz J and Daniel R. Development of a capillary electrophoresis assay based on free sulfate determination for the direct monitoring of sulfoesterase activity. *Analytical Biochemistry* 1999; **275**(1): 11–21.

Scott JE. Supramolecular organization of extracellular matrix glycosaminoglycans, *in vitro* and in the tissues. *FASEB Journal* 1992; **6**(9): 2639–2645.

Small DH, Mok SS, Williamson TG and Nurcombe V. Role of proteoglycans in neural development, regeneration, and the aging brain. *Journal of Neurochemistry* 1996; **67**(3): 889–899.

Srinivasan SR, Radhakrishnamurthy B, Dalferes ER Jr and Berenson GS. Determination of sulfate in glycosaminoglycans by gas–liquid chromatography. *Analytical Biochemistry* 1970; **35**(2): 398–404.

Sugahara K and Kitagawa H. Recent advances in the study of the biosynthesis and functions of sulfated glycosaminoglycans. *Current Opinion on Structural Biology* 2000; **10**(5): 518–527.

Suzuki A, Toyoda H, Toida T and Imanari T. Preparation and inhibitory activity on hyaluronidase of fully O-sulfated hyaluro-oligosaccharides. *Glycobiology* 2001; **11**(1): 57–64.

Tadano-Aritomi K, Hikita T, Suzuki A, Toyoda H, Toida T, Imanari T and Ishizuka I. Determination of lipid-bound sulfate by ion chromatography and its application to quantification of sulfolipids from kidneys of various mammalian species. *Journal of Lipid Research* 2001; **42**(10): 1604–1608.

Terho TT and Hartiala K. Method for determination of the sulfate content of glycosaminoglycans. *Analytical Biochemistry* 1971; **41**(2): 471–476.

Timerbaev AR. Recent advances and trends in capillary electrophoresis of inorganic ions. *Electrophoresis* 2002; **23**(22–23): 3884–3906.

Timerbaev AR. Capillary electrophoresis of inorganic ions: an update. *Electrophoresis* 2004; **25**(23–24): 4008–4031.

Toida T, Maruyama T, Suzuki A, Toyoda H, Imanari T and Linhardt RJ. Preparation and anticoagulant activity of fully O-sulphonated glycosaminoglycans. *International Journal of Biology and Macromoles* 1999; **26**(4): 233–241.

Tsuboi S, Isogai Y, Hada N, King JK, Hindsgaul O and Fukuda M. 6`-Sulfo sialyl Lex but not 6-sulfo sialyl Lex expressed on the cell surface supports L-selectin-mediated adhesion. *Journal of Biological Chemistry* 1996; **271**(44): 27213–3716.

Villanueva GB. Predictions of the secondary structure of antithrombin III and the location of the heparin-binding site. *Journal of Biological Chemistry* 1984; **259**(4): 2531–2536.

Werz DB and Seeberger PH. Carbohydrates as the next frontier in pharmaceutical research. *Chemistry* 2005; **11**(11): 3194–3206.

Wu XZ. Sulfated oligosaccharides and tumor: promoter or inhibitor? *Panminerva Medicine* 2006; **48**(1): 27–31.

Yoshida T, Yasuda Y, Mimura T, Kaneko Y, Nakashima H, Yamamoto N and Uryu T. Synthesis of curdlan sulfates having inhibitory effects *in vitro* against AIDS viruses HIV-1 and HIV-2. *Carbohydrate Research* 1995; **276**(2): 425–436.

Zaia J. On-line separations combined with MS for analysis of glycosaminoglycans. *Mass Spectrometry Review* 2009; **28**(2): 254–272.

# Heterologous down-regulation of angiotensin type 1 receptors by purinergic $P2Y_2$ receptor stimulation through S-nitrosylation of NF-κB

Motohiro Nishida[a], Mariko Ogushi[a], Reiko Suda[a], Miyuki Toyotaka[a], Shota Saiki[a], Naoyuki Kitajima[a], Michio Nakaya[a], Kyeong-Man Kim[b], Tomomi Ide[c], Yoji Sato[d], Kazuhide Inoue[e], and Hitoshi Kurose[a,1]

[a]Department of Pharmacology and Toxicology, Graduate School of Pharmaceutical Sciences, Kyushu University, Fukuoka 812-8582, Japan; [b]Department of Pharmacology, College of Pharmacy, Chonnam National University, Gwang-Ju 500-757 Korea; [c]Department of Cardiovascular Medicine, Graduate School of Medical Sciences, Kyushu University, Fukuoka 812-8582, Japan; [d]Division of Cellular and Gene Therapy Products, National Institute of Health Sciences, Tokyo 158-8501, Japan; and [e]Department of Molecular and System Pharmacology, Graduate School of Pharmaceutical Sciences, Kyushu University, Fukuoka 812-8582, Japan

Edited by Robert J. Lefkowitz, Duke University Medical Center/Howard Hughes Medical Institute, Durham, NC, and approved March 3, 2011 (received for review November 24, 2010)

**Cross-talk between G protein-coupled receptor (GPCR) signaling pathways serves to fine tune cellular responsiveness by neurohumoral factors. Accumulating evidence has implicated nitric oxide (NO)-based signaling downstream of GPCRs, but the molecular details are unknown. Here, we show that adenosine triphosphate (ATP) decreases angiotensin type 1 receptor ($AT_1R$) density through NO-mediated S-nitrosylation of nuclear factor κB (NF-κB) in rat cardiac fibroblasts. Stimulation of purinergic $P2Y_2$ receptor by ATP increased expression of inducible NO synthase (iNOS) through activation of nuclear factor of activated T cells, NFATc1 and NFATc3. The ATP-induced iNOS interacted with p65 subunit of NF-κB in the cytosol through flavin-binding domain, which was indispensable for the locally generated NO-mediated S-nitrosylation of p65 at Cys38. β-Arrestins anchored the formation of p65/IκBα/β-arrestins/iNOS quaternary complex. The S-nitrosylated p65 resulted in decreases in NF-κB transcriptional activity and $AT_1R$ density. In pressure-overloaded mouse hearts, ATP released from cardiomyocytes led to decrease in $AT_1R$ density through iNOS-mediated S-nitrosylation of p65. These results show a unique regulatory mechanism of heterologous regulation of GPCRs in which cysteine modification of transcriptional factor rather than protein phosphorylation plays essential roles.**

angiotensin receptor | $Ca^{2+}$ signaling | calcineurin | signaling complex | posttranslational modification

G protein-coupled receptors (GPCRs) are the largest family of cell-surface receptors, which play a critical role in regulating multiple physiological functions (1, 2). Abnormal activation or up-regulation of GPCRs is a major cause of various diseases (3), and about 40% of drugs that are widely used for therapeutic treatment all over the world may directly or indirectly target GPCRs.

An important adaptive response of the cell against multiple extracellular stimuli is receptor desensitization, which refers to the reduction of receptor responsiveness despite continuing agonist stimulation. GPCRs have developed elaborate means of turning off signal (4). One mechanism for desensitization is receptor down-regulation, which refers to the net loss of receptors from the cell by a decrease in receptor synthesis, a destabilization of receptor mRNA, or an increase in receptor degradation (4, 5).

Two major patterns of down-regulation have been characterized; homologous (or agonist specific) down-regulation and heterologous (or agonist nonspecific) down-regulation (6). The homologous down-regulation indicates that stimulation of one GPCR over time by the agonist reduces expression levels of the same GPCR, without substantial effect on other GPCRs present in the same cell. In contrast, heterologous down-regulation indicates that stimulation of one GPCR reduces expression levels of different GPCR. Although the molecular mechanism of homologous down-regulation has been well analyzed using β-adrenergic receptors (βARs) (4, 5), the mechanism(s) underlying heterologous down-regulation is largely unknown.

Angiotensin (Ang) II is a major bioactive polypeptide, and improper regulation of Ang II induces various cardiovascular diseases, including hypertension, cardiac hypertrophy, fibrosis, apoptosis, and arrhythmia (7). Most of known physiological and pathological effects of Ang II are mediated via the angiotensin type 1 receptor ($AT_1R$). In fact, aberrant expression of $AT_1R$ has been shown to have pathophysiological relevance in cell culture, animal studies, and clinical interventional trials (8). Ang II decreases $AT_1R$ expression level through destabilization of $AT_1R$ mRNA (9), suggesting the involvement of homologous down-regulation processes. In addition, the expression of $AT_1Rs$ could be regulated by various factors, including cytokines, growth factors, and reactive oxygen species (ROS). However, heterologous down-regulation of $AT_1Rs$ through different GPCRs has not been reported.

It is well established that nitric oxide (NO) regulates a diverse array of signal transduction pathways, acting in significant part through the covalent modification of cysteine (Cys) thiols (S-nitrosylation) that are found at active or allosteric sites of proteins (10). Several transmembrane-spanning receptors and their downstream signaling molecules could be modified by NO, including NMDA receptor (11), GPCR kinase 2 (12), β-arrestin (13), and G proteins (14, 15). Although exposure of excessive NO has been reported to decrease $AT_1R$ density (16), the molecular details and its physiological significance are still unknown.

During the analysis of the roles of $Ca^{2+}$ signaling in cardiac fibroblasts, we noticed that the pretreatment with adenosine triphosphate (ATP) selectively suppressed $AT_1R$-stimulated $Ca^{2+}$ response. We have found that stimulation of $P2Y_2$ receptor with ATP down-regulates $AT_1R$ signaling through expression of inducible NO synthase (iNOS) without nuclear factor κB (NF-κB) activation. Down-regulation of $AT_1R$ requires functional interaction of NF-κB with iNOS, and the locally generated NO mediates cysteine modification (S-nitrosylation) of NF-κB, leading to suppression of $AT_1R$ transcription rate.

Author contributions: M. Nishida designed research; M. Nishida, M.O., R.S., M.T., S.S., N.K., T.I., and Y.S. performed research; K.I. contributed new reagents/analytic tools; M. Nishida, M.O., R.S., M.T., S.S., M. Nakaya, and Y.S. analyzed data; and M. Nishida, K.-M.K., and H.K. wrote the paper.

The authors declare no conflict of interest.

This article is a PNAS Direct Submission.

[1]To whom correspondence should be addressed. E-mail: kurose@phar.kyushu-u.ac.jp.

This article contains supporting information online at www.pnas.org/lookup/suppl/doi:10.1073/pnas.1017640108/-/DCSupplemental.

## Results

**$P2Y_2$ Receptor Stimulation Selectively Down-Regulates $AT_1R$ Signaling.** In a normal heart, two-thirds of the cell population is composed of cardiac fibroblasts. Expression level of $AT_1R$ in rat neonatal cardiac fibroblasts is more than fivefold higher than that in rat neonatal cardiomyocytes (65 ± 12 fmol/mg protein), and $AT_1R$ signaling in cardiac fibroblasts has been implicated in the development of cardiac fibrosis (17). We have previously reported that treatment with Ang II increases activity of nuclear factor of activated T cells (NFAT), a $Ca^{2+}$-dependent transcriptional factor that is predominantly regulated by calcineurin, both in cardiac myocytes and fibroblasts (18, 19). Activation of NFAT has been implicated in the development of cardiac hypertrophy (20), but the role of NFAT in cardiac fibroblasts is not fully known. Therefore, we first examined the relationship between NFAT activity and $AT_1R$ signaling in cardiac fibroblasts. We found that treatment with ATP more potently increased NFAT activity than Ang II, the endogenous ligand of $G_q$PCR (Fig. 1 *A* and *B*). Purinergic receptors are classified into two families, P2X and P2Y (21). P2X receptors are ligand-gated channels. P2Y receptors are G protein-coupled receptors, and divided into eight subtypes. Purinergic signaling has been implicated in inflammatory responses of various systems (22, 23), and we have also reported that extracellular nucleotides trigger pressure overload-induced cardiac fibrosis in mice (24). The ATP-induced increases in intracellular $Ca^{2+}$ concentration ($[Ca^{2+}]_i$) and NFAT activity were completely suppressed by the inhibition of phospholipase C (PLC) and knockdown of $P2Y_2$ receptor ($P2Y_2R$), but not by inhibition of $P2Y_1R$ and $P2Y_6R$ (Fig. S1). These results suggest that $P2Y_2R$ predominantly regulates ATP-induced activation of $Ca^{2+}$ signaling in rat cardiac fibroblasts.

The treatment with ATP for 24 h resulted in a decrease in expression levels of $AT_1R$ mRNA and protein (Fig. 1 *C* and *D*), which was abolished by cyclosporine A, a specific calcineurin inhibitor. In addition, expression of Cain, a specific inhibitory peptide of calcineurin (25), also canceled the ATP-induced decrease in $AT_1R$ density and $AT_1R$-induced signaling (Fig. S2 *A–C*). Expression of constitutively active mutant of NFAT4 (NFAT-CA) inhibited $AT_1R$ mRNA expression (Fig. 1*C*), indicating that calcineurin-NFAT signaling mediates $AT_1R$ down-regulation. As $AT_1R$ couples with $G_q$ family proteins, the Ang II-induced transient increase in $[Ca^{2+}]_i$ was measured as an index of the magnitude of $AT_1R$ signaling. Pretreatment with ATP or overexpression of NFAT-CA significantly decreased the Ang II-induced maximal $[Ca^{2+}]_i$ increases without changing $EC_{50}$ values (Fig. 1 *E* and *F*). There are four NFAT isoforms responsive to increase in $[Ca^{2+}]_i$ (26). Among them, NFATc1 participates in cardiac valve development and NFATc3 participates in the development of cardiac hypertrophy. Treatment of cardiac fibroblast with ATP induced nuclear translocation of NFATc1 and NFATc3, but not NFATc2 (Fig. S2 *D* and *E*). We could not detect the expression of NFATc4 proteins. These results suggest that stimulation of $G_q$-coupled $P2Y_2$ receptor by ATP induces heterologous down-regulation of $G_q$-coupled $AT_1R$ through activation of NFATc1 and NFATc3 in rat cardiac fibroblasts. Although $P2Y_2R$ can be stimulated not only by ATP but also by ADP and UTP (21), ATP maximally increased NFAT activity and decreased $AT_1R$ signaling (Fig. S3). However, endothelin-1 and bradykinin, which signal through $G_q$ (27), failed to imitate ATP both in NFAT activation and inhibition of $G_q$ signaling, suggesting that the ATP-mediated suppression of $AT_1R$ signaling is likely to correlate with its potential to increase NFAT activity. Furthermore, pretreatment with Ang II did not affect the ATP-induced $Ca^{2+}$ response (Fig.S3 *C* and *D*), suggesting that ATP specifically induces heterologous down-regulation of $AT_1R$ signaling but not vice versa.

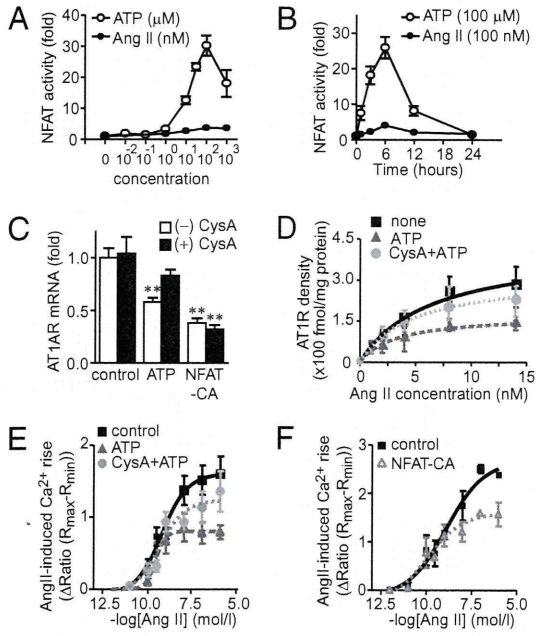


**Fig. 1.** ATP decreases $AT_1R$ density through NFAT activation. (*A*) Concentration-dependent NFAT activation induced by ATP and Ang II in rat neonatal cardiac fibroblasts. Cells were treated with indicated concentration of ATP or Ang II for 6 h. (*B*) Time courses of NFAT activation induced by ATP and Ang II. (*C*) Changes in $AT_{1A}R$ mRNA expression levels by the treatment with ATP (100 μM) for 24 h or overexpression of NFAT-CA in the presence or absence of CysA (100 ng/mL). Cells were treated with CysA 10 min before ATP stimulation. (*D*) Changes in $AT_1R$ density induced by ATP (100 μM) for 24 h with or without CysA ($n$ = 4–6). (*E*) Peak increases in $[Ca^{2+}]_i$ induced by Ang II stimulation in ATP-treated or ATP/CysA-treated cardiac fibroblasts. Cells were treated with CysA (100 ng/mL) 10 min before stimulation of ATP (100 μM) for 24 h. (*F*) Peak $[Ca^{2+}]_i$ increases induced by Ang II in LacZ (control)- and NFAT-CA-expressing cardiac fibroblasts. Cells were infected with Ad-LacZ or Ad-NFAT-CA for 48 h ($n$ = 63–99). $^{**}P < 0.01$.

**ATP Decreases $AT_1R$ Density Through iNOS Expression.** We next examined the mechanism of $AT_1R$ down-regulation by NFAT activation. Because the mRNA stability of $AT_1R$ was not decreased by ATP treatment (Fig. S3*E*), its effects on the $AT_1R$ transcription rate were further studied. NF-κB has been reported to participate in $AT_1R$ up-regulation induced by cytokines or bacterial toxin (28, 29), and inhibition of NF-κB significantly suppressed $AT_1R$ transcription rate and $AT_1R$ density (Fig. S4). Thus, basal activity of $AT_1R$ transcription may be mainly regulated by NF-κB. In addition, NO has been reported to decrease NF-κB and $AT_1R$ transcription (16). Thus, NO may mediate ATP-induced $AT_1R$ down-regulation. Treatment with ATP induced a time-dependent decrease in expression of luciferase from $AT_1R$ promoter, as well as a decrease in NF-κB–dependent luciferase activity (Fig. 2*A*). The ATP-induced suppression of $AT_1R$ transcription rate was abolished by N(G)-nitro-L-arginine methyl ester (L-NAME) or *N*-(3-(aminomethyl)benzyl)acetamidine (1400W), a specific inhibitor of iNOS (Fig. 2*B*). Treatment with 1400W canceled the ATP-induced decrease in $AT_1R$ density and suppression of $AT_1R$-stimulated $Ca^{2+}$ response (Fig. 2 *C–E*). In addition, knockdown of iNOS, but not endothelial NOS (eNOS), abolished the ATP-induced suppression of $Ca^{2+}$ response by $AT_1R$ stimulation (Fig. 2*F*), suggesting that iNOS mediates ATP-induced $AT_1R$ down-regulation. It is generally accepted that NF-κB predominantly regulates the expression level of iNOS proteins (30). However, it has also been reported that iNOS proteins are induced by the constitutive activation of calcineurin-NFAT signaling in cardiomyocytes (31). In accordance with this, the expression of a constitutively active mutant

PHARMACOLOGY

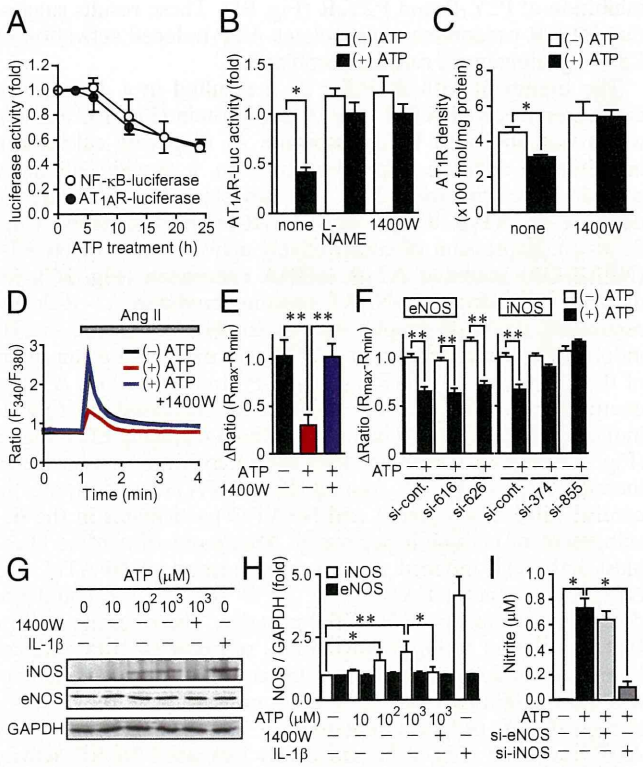


**Fig. 2.** iNOS mediates ATP-induced $AT_1R$ down-regulation. (*A*) Time-dependent suppression of NF-κB-dependent and $rAT_{1A}R$ promoter-dependent luciferase activities induced by ATP (100 μM). (*B*) Effects of iNOS inhibitors on the ATP-induced decrease in $rAT_{1A}R$ promoter activity. Cells were treated with L-NAME (100 μM) or 1400W (10 μM) 10 min before sitmulation with ATP (100 μM) for 24 h. (*C*) Effects of 1400W on the ATP-induced decrease in $AT_1R$ protein expression ($n$ = 3–5). (*D*) Time courses of $AT_1R$-stimulated increases in $[Ca^{2+}]_i$ in cardiac fibroblasts pretreated with ATP or ATP and 1400W. (*E*) Peak increases in $[Ca^{2+}]_i$ induced by Ang II (100 nM). Cells were treated with 1400W (10 μM) 10 min before sitmulation with ATP (100 μM) for 24 h. (*F*) Peak increases in $[Ca^{2+}]_i$ induced by Ang II in siRNA-transfected cardiac fibroblasts pretreated with or without ATP (100 μM) for 24 h. Cells were treated with ATP 48 h after transfection with siRNAs for eNOS and iNOS. ($n$ = 42–78) (*G* and *H*) Changes in expressions of iNOS, eNOS and GAPDH proteins by the stimulation with ATP and IL-1β (1 ng/mL) for 24 h in the presence or absence of 1400W (10 μM). (*I*) Effects of siRNAs for eNOS or iNOS on the ATP-induced nitrite production. Cells were treated with ATP (100 μM) for 24 h. ($n$ = 3). $^*P < 0.05$, $^{**}P < 0.01$.

of NFAT (NFAT-CA) decreased $AT_1R$-stimulated $Ca^{2+}$ response, which was completely abolished by the treatment with L-NAME or 1400W (Fig. S5). ATP-stimulated increase of iNOS proteins was completely suppressed by 1400W (Fig. 2 *G* and *H*). In addition, ATP-induced NO production was completely suppressed by the knockdown of iNOS, but not eNOS (Fig. 2*I*). As ATP strongly induced NFAT activity, NFAT-dependent iNOS expression may mediate the ATP-induced down-regulation of $AT_1R$ in cardiac fibroblasts.

**Requirement of S-Nitrosylation of p65 for ATP-Induced $AT_1R$ Down-Regulation.** As the treatment with protein kinase G (PKG) inhibitor (KT5823) did not cancel the ATP-induced down-regulation of $AT_1R$ signaling, and a cGMP analog (8-bromo-cGMP) did not induce $AT_1R$ down-regulation (Fig. S5 *A* and *B*), NO may suppress $AT_1R$ transcription in a cGMP-independent manner. S-nitrosylation has been recently recognized as a new NO-based but cGMP-independent signaling regulating several cardiovascular functions (10). Dimers of NF-κB proteins are composed of five transcriptional factors: p50, p52, p65, Rel, and RelB, which all share an N-terminal Rel homology domain (32). Among them, S-nitrosylation of p50 and p65 has been reported to participate in iNOS-induced decrease in NF-κB transcriptional activity (33, 34). We next examined whether S-nitrosylation participates in ATP-induced $AT_1R$ down-regulation. It was reported that a conserved Cys within the DNA-binding site of the Rel homology domain is the site of S-nitrosylation (33). Thus, we constructed Cys mutants of p65 (p65-C38S) and p50 (p50-C62S) to examine which Cys is involved in ATP-induced $AT_1R$ down-regulation. Overexpression of wild-type p65 (p65-WT) and p65-C38S enhanced the $AT_1R$-stimulated increases in $[Ca^{2+}]_i$, suggesting that transcriptional activity of p65 is not affected by substitution of Ser for Cys. The ATP-induced suppression of $AT_1R$ signaling normally occurred in vector- and p65-WT–expressing cardiac fibroblasts but was completely abolished in p65-C38S–expressing cardiac fibroblasts (Fig. 3 *A* and *B*). Substitution of Ser for other eight Cys residues of p65 did not affect the ATP-induced suppression of $AT_1R$ signaling (Fig. S6), suggesting that Cys38 of p65 participates in ATP-induced S-nitrosylation and $AT_1R$ down-regulation. In contrast, expression of p50-C62S did not abolish the suppression of $AT_1R$ signaling induced by ATP (Fig. 3 *C* and *D*). Although p50 essentially lacks transactivation domain (32), overexpression of p50-WT and p50-C62S enhanced the $AT_1R$-stimulated $Ca^{2+}$ responses, suggesting that p50 does not mediate ATP-induced suppression of $AT_1R$ signaling. It has been previously reported that phosphorylation of p65 at Ser468 reduces basal NF-κB activity (35). However, treatment with ATP did not increase the phosphorylation

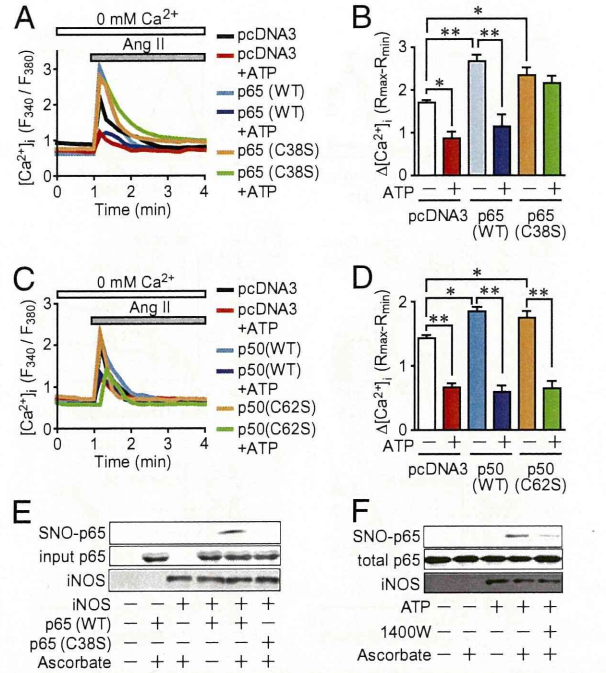


**Fig. 3.** S-nitrosylation of p65 mediates ATP-induced $AT_1R$ down-regulation. (*A*) Time courses of $Ca^{2+}$ responses induced by Ang II (100 nM) in vector, p65 (WT) or p65 (C38S)-overexpressing cardiac fibroblasts. Cells were pretreated with ATP (100 μM) for 24 h. (*B*) Peak increases in $[Ca^{2+}]_i$ induced by Ang II ($n$ = 41–68). (*C*, *D*) Time courses (*C*) and peak changes (*D*) of $Ca^{2+}$ responses induced by Ang II in vector, p50 (WT) or p50 (C62S)-expressing fibroblasts ($n$ = 44–72). (*E*) S-nitrosylation of Cys38 of p65 in p65 and iNOS-expressing HEK293 cells. Cell lysates were incubated with ascorbate (1 mM) for 1 h at 25 °C in the dark room. (*F*) S-nitrosylation of p65 and iNOS expression induced by ATP stimulation in cardiac fibroblasts. Cells were treated with 1400 W (10 μM) 10 min before stimulation with ATP (100 μM) for 24 h. Cell lysates were incubated with ascorbate (1 mM) for 1 h at 25 °C in the dark room ($n$ = 3). $^*P < 0.05$, $^{**}P < 0.01$.

level of p65 at Ser468, and substitution of Ala for Ser468 did not affect the suppression of $AT_1R$-stimulated $Ca^{2+}$ response induced by ATP (Fig. S6 *D–F*). Thus, phosphorylation of p65 is not involved in ATP-induce $AT_1R$ down-regulation. The expression of iNOS proteins induced S-nitrosylation of p65 at Cys38 in HEK293 cells (Fig. 3*E*), and the treatment of cardiac fibroblasts with ATP induced S-nitrosylation of p65 in an iNOS-dependent manner (Fig. 3*F*). These results suggest that S-nitrosylation of p65 at Cys38 participates in the ATP-induced $AT_1R$ down-regulation in cardiac fibroblasts.

**Requirement of the Interaction Between iNOS and p65 for ATP-Induced $AT_1R$ Down-Regulation.** The extent of iNOS induction by ATP was smaller than that by IL-1β, a potent activator of NF-κB signaling (Fig. 2 *G* and *H*). This apparent discrepancy may be explained by the differences in the colocalization between p65 and iNOS, which is predominantly expressed in the cytosol (33), in ATP-, and IL-1β–treated cells. In iNOS- and p65-overexpressing HEK293 cells, both p65-WT and p65-C38S interacted with iNOS (Fig. 4*A*). In addition, iNOS induced by ATP, but not eNOS, interacted with p65 in rat cardiac fibroblasts, which was completely suppressed by cyclosporine A (Fig. 4*B*). Although cotreatment with S-nitrosoglutathione (GSNO) (1 mM) significantly enhanced ATP-induced S-nitrosylation of p65, GSNO did not affect the ATP-induced interaction between p65 and iNOS (Fig. S7). These results suggest that p65 associates with iNOS independently of Cys modification. In the resting condition, p65 was expressed both in the cytosol and nucleus, whereas iNOS was hardly detected in cardiac fibroblasts (Fig. 4*C*). Treatment with ATP induced expression of iNOS in the cytosol without affecting the subcellular localization of p65, resulting in colocalization of p65 and iNOS in the cytosol. In contrast, IL-1β markedly increased expression levels of iNOS and induced continuous translocation of p65 into the nucleus, resulting in little colocalization between p65 and iNOS. We next examined which domain of iNOS is required for the interaction with p65. As iNOS has N-terminal oxygenase domain and C-terminal reductase domain (36), and the C-terminal domain has flavin-binding domain and NADPH-binding domain, we constructed four fragments of iNOS (Fig. 4 *D* and *E*). In HEK293 cells expressing p65 and each iNOS fragment (Fr-I–Fr-IV), p65 was interacted with Fr-III only, which contains flavin-binding domain (Fig. 4*F*). Furthermore, expression of cardiac fibroblasts with Fr-III completely blocked the ATP-induced interaction of p65 with iNOS and suppression of $AT_1R$-stimulated $Ca^{2+}$ response (Fig. 4 *G* and *H*). These results suggest that iNOS induced by ATP stimulation interacts with p65 in the cytosol through flavin-binding domain, which is required for S-nitrosylation of p65 and which decreases its activity in rat cardiac fibroblasts.

Previous reports have clearly shown that β-arrestins associate with NOS and IκBα (13, 37–39). As the IκBα interacts with NF-κB p65 subunit, ATP may induce the formation of quaternary complex of iNOS/β-arrestin/IκBα/p65 in cardiac fibroblasts. To verify this hypothesis, we further examined whether knockdown of β-arrestin(s) cancels the ATP-induced p65-iNOS interaction. Knockdown of β-arrestin2 significantly suppressed the down-regulation of $AT_1R$ signaling (Fig. S8). The β-arrestins were predominantly expressed in the cytosol of cardiac fibroblasts, and the ATP-induced colocalization of p65 with iNOS was diminished by β-arrestin2 knockdown. In addition, p65 actually interacted not only with iNOS, but also IκBα and β-arrestin2 in ATP-pretreated cardiac fibroblasts, which was diminished by β-arrestin2 knockdown. Although knockdown of β-arrestin1 also suppressed the p65-iNOS colocalization and down-regulation of $AT_1R$ signaling induced by ATP pretreatment, the magnitude of suppression was smaller than that of β-arrestin2. These results

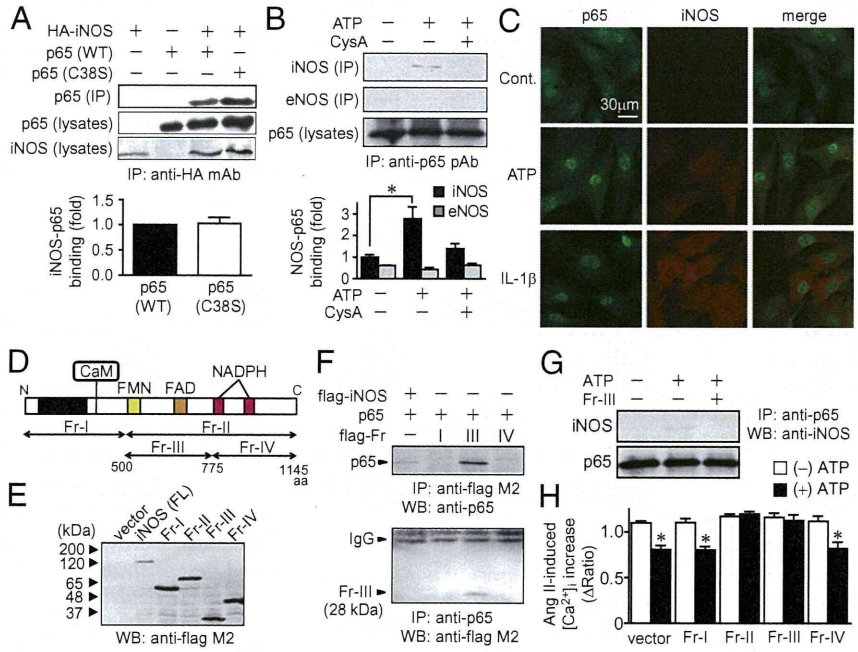


**Fig. 4.** ATP-induced iNOS interacts with p65. (*A*) Association of iNOS proteins with p65 (WT or C38S) in p65 and iNOS-expressing HEK293 cells. IP: immunoprecipitation, WB: Western blotting. HA-tagged iNOS proteins were immunoprecipitated with anti-HA antibody (IP), and combined p65 proteins were detected by Western blotting. Expression levels of p65 and iNOS were also confirmed using total cell lysates (lysates). (*B*) ATP stimulation-dependent interaction of p65 with iNOS in cardiac fibroblasts. Cells were treated with ATP (100 μM) for 24 h in the presence or absence of CysA (100 ng/mL). Native p65 proteins were immunoprecipitated with anti-p65 antibody (IP) ($n = 3$). (*C*) Localization of p65 and iNOS proteins in cardiac fibroblasts stimulated with ATP (100 μM) or IL-1β (1 ng/mL) for 24 h. (*D*) Structure of iNOS fragments (Fr-I – Fr-IV). (*E*) Expression of flag-tagged iNOS fragments. FL; full length. (*F*) Interaction of p65 with Fr-III. (*G*) Effects of Fr-III on the ATP-induced interaction of p65 with iNOS ($n = 3$). (*H*) Effects of iNOS fragments on the ATP-induced down-regulation of $AT_1R$ signaling ($n = 39–62$). $^*P < 0.05$.

indicate that β-arrestins mediate the ATP-induced formation of quaternary complex of iNOS/β-arrestins/IκBα/p65 in the cytosol of cardiac fibroblasts. Although β-arrestins participate in GPCR-stimulated activation of extracellular signal-regulated kinase (ERK), treatment with ERK inhibitors (U0126 and PD98059) did not cancel the ATP-induced down-regulation of $AT_1R$ signaling (Fig. S9). Thus, β-arrestins may participate in ATP-induced $AT_1R$ down-regulation through anchoring the interaction between p65 and iNOS proteins.

**ATP Mediates Down-Regulation of $AT_1R$ Signaling in Pressure-Overloaded Mouse Hearts.** We finally examined whether ATP-induced $AT_1R$ down-regulation occurred in vivo. We have previously reported that nucleotides (such as ATP and UDP) released from cardiac myocytes stimulate the production of fibrotic genes, which activate the production of collagen in cardiac fibroblasts in pressure overload-induced mice (24). As nucleotides are released from cardiac myocytes and the expression levels of $AT_1Rs$ in cardiac fibroblasts are higher than those in cardiac myocytes, both cardiac myocytes and fibroblasts were cocultured on a silicone rubber dish. Mechanical stretch that stimulates nucleotides release from cardiac myocytes (24) decreased $AT_1R$ density, which was canceled by pretreatment with L-NAME (Fig. 5*A*). As expected, inhibition of $P2Y_2R$ by PPADS or $P2Y_2R$ siRNA completely abolished mechanical stretch-induced $AT_1R$ down-regulation. Mechanical stretch of cardiac cells induced ATP release, which leads to NO production in $P2Y_2R$ and iNOS-dependent manners (Fig. 5 *B* and *C*). Furthermore, 6 wk of transverse aortic constriction (TAC) induced significant increases in iNOS mRNA and protein levels and S-nitrosylation of p65, which were completely suppressed by the treatment with suramin, a P2 receptor antagonist (Fig. 5 *D* and *E*). Pressure overload also increased expression levels of eNOS proteins, but this increase was not affected by suramin. In addition, 6 wk of TAC decreased expression levels of $AT_1R$ mRNA and proteins, which were also abolished by suramin treatment (Fig. 5 *E* and *F*). Furthermore, pressure overload-induced S-nitrosylation of p65 was diminished in iNOS knockout mouse hearts (Fig. 5 *G* and *H*) and in 1400W-treated mouse hearts (Fig. S10). These results suggest that mechanical stretch-induced ATP release causes $AT_1R$ down-regulation through iNOS-dependent S-nitrosylation of p65 in pressure overloaded mice.

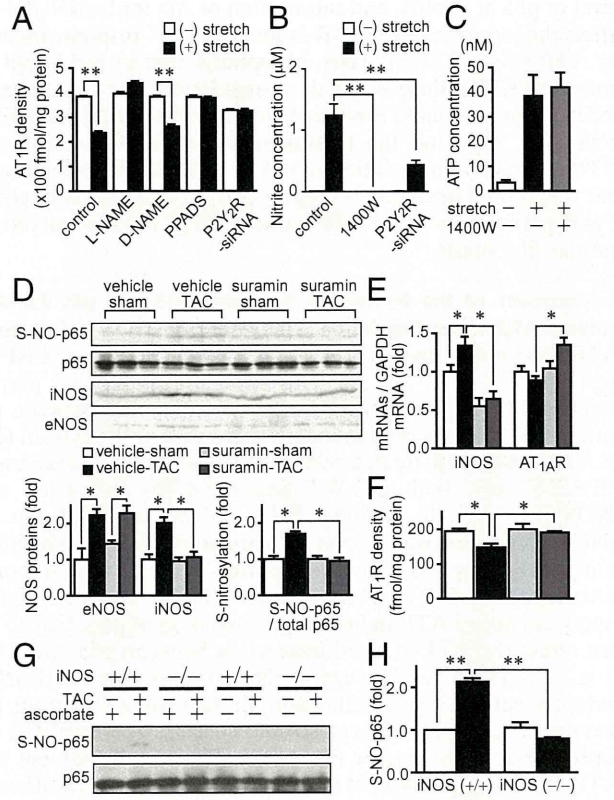


**Fig. 5.** Mechanical stretch induces $AT_1R$ down-regulation through ATP-induced S-nitrosylation of NF-κB. (*A*) Effects of L-NAME (100 μM), D-NAME (100 μM), PPADS (100 μM), and $P2Y_2R$ siRNA on mechanical stretch-induced decrease in $AT_1R$ density in rat cardiac myocytes. (*B*) Effects of 1400W (10 μM) and $P2Y_2R$ siRNA on mechanical stretch-induced nitrite production. (*C*) Effects of 1400W on mechanical stretch-induced ATP release ($n$ = 3–5). (*D–F*) S-nitrosylation of p65, changes in expression of iNOS, p65, eNOS and $AT_1R$ proteins induced by pressure overload in the presence or absence of suramin in mouse hearts. (*E*) Changes in iNOS and $AT_{1A}R$ mRNAs induced by TAC. (*F*) Changes in $AT_1R$ density induced by TAC in the presence or absence of suramin ($n$ = 3–6). (*G* and *H*) S-nitrosylation of p65 induced by pressure overload in wild type (+/+) and iNOS-knockout (–/–) mouse hearts. Tissue lysates were treated with or without ascorbate (1 mM) for 1 h ($n$ = 3). $^*P < 0.05$, $^{**}P < 0.01$.

## Discussion

A large number of studies have shown that a wide range of physiological and pathological stimuli modulate $AT_1R$ expression in a number of cell types and tissues (40). We first demonstrated that ATP induces down-regulation of $AT_1R$ signaling in rat cardiac fibroblasts. Extracellular ATP in the cardiovascular system may be originated from various cellular sources: perivascular sympathetic nerve endings, myocytes, endothelial cells, and inflammatory cells (14). We found that mechanical stretch-induced ATP release decreases $AT_1R$ density in mouse hearts with pressure overload (Fig. 5). Although both ATP and Ang II are believed to function as an inflammatory factor (41), our results suggest that $P2Y_2R$-stimulated iNOS expression negatively regulates Ang II-mediated inflammatory response of the heart. We have previously reported that nucleotides released from cardiac myocytes activate $P2Y_6R$ of cardiac myocytes and induce fibrotic genes (24). In addition, Braun et al. has recently reported that $P2Y_2R$ stimulation by UTP induces fibrotic responses of cardiac fibroblasts (42). Thus, extracellular nucleotides contribute to cardiac fibrosis at least two independent pathways: one is induction of fibrotic genes in cardiac myocytes through $P2Y_6R$ and another is iNOS-mediated signaling in cardiac fibroblasts through $P2Y_2R$. The pathophysiological roles of $P2Y_2R$ signaling in the heart are still unclear, but our findings will provide a unique insight into the cross-talk between purinergic signaling and Ang II signaling in cardiovascular systems.

We revealed that local production of NO induces S-nitrosylation of NF-κB p65 and suppresses $AT_1R$ transcription leading to down-regulation of $AT_1R$. Several reports have suggested the involvement of S-nitrosylation in NO-dependent (but cGMP independent) regulation of β-adrenergic receptor desensitization (12, 13). Most studies have shown the involvement of S-nitrosylation in GPCR desensitization by exposing excessive concentrations of NO to the cell. However, GRK2 is endogenously S-nitrosylated and levels are lower in eNOS null animals and higher in $GSNOR^{-/-}$ animals. Furthermore, receptor internalization in cellular assays and desensitization in situ are regulated by endogenously derived NO. We also found that endogenous S-nitrosylation of NF-κB p65 requires the formation of iNOS/β-arrestins/IκBα/p65 quaternary complex in the cytosol. This finding emphasizes the fact that β-arrestins play a key mediator in NO-based signaling. Although IL-1β potently induces expression of iNOS, IL-1β did not suppress NF-κB activity. This may be explained by the evidence that p65 was not colocalized with iNOS by IL-1β stimulation (Fig. 4). Thus, the complex formation between NO donor and acceptor is a critical factor of spatiotemporal regulation of NO signaling induced by ATP stimulation.

In conclusion, we reveal that S-nitrosylation of p65 is required for heterologous down-regulation of $G_q$-coupled $AT_1R$ by another $G_q$-coupled $P2Y_2R$ stimulation. Although it is generally thought that heterologous regulation of GPCRs is mediated by second messenger-activated kinases, heterologous down-regulation of $AT_1R$ by ATP did not require the kinase activation in which cysteine modification of transcriptional factor plays essential roles. Our findings will provide a unique insight into cross-talk between GPCR signaling pathways.

## Materials and Methods

Materials, recombinant adenoviruses, and culture of cardiac fibroblasts, measurement of NF-κB-luciferase and $AT_1R$-luciferase activity, measurement of extracellular ATP concentration and NO production, measurement of $AT_1R$ and iNOS expressions, quantification of intracellular $Ca^{2+}$ concentration, S-nitrosylation biotin switch assay, immunoprecipitation, and confocal visualization of NF-κB p65 subunit and iNOS proteins are described in *SI Materials and Methods*.

**Animals and TAC Surgery.** All protocols using mice and rats were approved by the guidelines of Kyushu University. Mice with a homozygous deletion of the iNOS gene were purchased from The Jackson Laboratory. TAC surgery was performed on 6-wk-old male C57BL/6J mice (24). A mini-osmotic pump (Alzet) filled with vehicle (saline), suramin or 1400W was implanted intraperitoneally 3 d after TAC into 6-wk-old male C57BL/6J mice.

**Statistical Analysis.** The results are presented as mean ± SEM from at least three independent experiments. The representative data of time course experiments were plotted from one of three similar experiments that were performed with more than 20 cells. Statistical comparisons were made with two-tailed Student's *t* test or one way analysis of variance followed by Student-Newman-Keuls procedure, with significance imparted at $P < 0.05$.

**ACKNOWLEDGMENTS.** We thank K. Watanabe and A. Uemura for TAC operation. This study was supported by grants from Grant-in-Aid for Scientific Research on Innovative Areas (to M. Nishida); from the Ministry of Education, Culture, Sports, Science, and Technology of Japan (to M. Nishida, M. Nakaya, and H.K.); and from the Naito Foundation and Mochida Memorial Foundation (to M. Nishida).

1. Pierce KL, Premont RT, Lefkowitz RJ (2002) Seven-transmembrane receptors. *Nat Rev Mol Cell Biol* 3:639–650.
2. Rockman HA, Koch WJ, Lefkowitz RJ (2002) Seven-transmembrane-spanning receptors and heart function. *Nature* 415:206–212.
3. Philipp M, Hein L (2004) Adrenergic receptor knockout mice: Distinct functions of 9 receptor subtypes. *Pharmacol Ther* 101:65–74.
4. Lefkowitz RJ (1998) G protein-coupled receptors. III. New roles for receptor kinases and β-arrestins in receptor signaling and desensitization. *J Biol Chem* 273: 18677–18680.
5. Pitcher JA, Freedman NJ, Lefkowitz RJ (1998) G protein-coupled receptor kinases. *Annu Rev Biochem* 67:653–692.
6. Chuang TT, Iacovelli L, Sallese M, De Blasi A (1996) G protein-coupled receptors: Heterologous regulation of homologous desensitization and its implications. *Trends Pharmacol Sci* 17:416–421.
7. de Gasparo M, Catt KJ, Inagami T, Wright JW, Unger T (2000) International union of pharmacology. XXIII. The angiotensin II receptors. *Pharmacol Rev* 52:415–472.
8. Wassman S, Nickenig G (2006) Pathophysiological regulation of the AT1-receptor and implications for vascular disease. *J Hypertens* 24:515–521.
9. Nickenig G, et al. (2002) Destabilization of AT(1) receptor mRNA by calreticulin. *Circ Res* 90:53–58.
10. Lima B, Forrester MT, Hess DT, Stamler JS (2010) S-nitrosylation in cardiovascular signaling. *Circ Res* 106:633–646.
11. Jaffrey SR, Erdjument-Bromage H, Ferris CD, Tempst P, Snyder SH (2001) Protein S-nitrosylation: A physiological signal for neuronal nitric oxide. *Nat Cell Biol* 3:193–197.
12. Whalen EJ, et al. (2007) Regulation of β-adrenergic receptor signaling by S-nitrosylation of G-protein-coupled receptor kinase 2. *Cell* 129:511–522.
13. Ozawa K, et al. (2008) S-nitrosylation of β-arrestin regulates β-adrenergic receptor trafficking. *Mol Cell* 31:395–405.
14. Lander HM, et al. (1996) Redox regulation of cell signalling. *Nature* 381:380–381.
15. Nishida M, et al. (2002) Activation mechanism of $G_i$ and $G_o$ by reactive oxygen species. *J Biol Chem* 277:9036–9042.
16. Ichiki T, et al. (1998) Downregulation of angiotensin II type 1 receptor gene transcription by nitric oxide. *Hypertension* 31:342–348.
17. Porter KE, Turner NA (2009) Cardiac fibroblasts: At the heart of myocardial remodeling. *Pharmacol Ther* 123:255–278.
18. Onohara N, et al. (2006) TRPC3 and TRPC6 are essential for angiotensin II-induced cardiac hypertrophy. *EMBO J* 25:5305–5316.
19. Fujii T, et al. (2005) Galpha12/13-mediated production of reactive oxygen species is critical for angiotensin receptor-induced NFAT activation in cardiac fibroblasts. *J Biol Chem* 280:23041–23047.
20. Molkentin JD, et al. (1998) A calcineurin-dependent transcriptional pathway for cardiac hypertrophy. *Cell* 93:215–228.
21. Erlinge D, Burnstock G (2008) P2 receptors in cardiovascular regulation and disease. *Purinergic Signal* 4:1–20.
22. Koizumi S, et al. (2007) UDP acting at $P2Y_6$ receptors is a mediator of microglial phagocytosis. *Nature* 446:1091–1095.
23. Seye CI, et al. (2002) Functional $P2Y_2$ nucleotide receptors mediate uridine 5′-triphosphate-induced intimal hyperplasia in collared rabbit carotid arteries. *Circulation* 106:2720–2726.
24. Nishida M, et al. (2008) P2Y6 receptor-Galpha12/13 signalling in cardiomyocytes triggers pressure overload-induced cardiac fibrosis. *EMBO J* 27:3104–3115.
25. Lai MM, Burnett PE, Wolosker H, Blackshaw S, Snyder SH (1998) Cain, a novel physiologic protein inhibitor of calcineurin. *J Biol Chem* 273:18325–18331.
26. Wu H, Peisley A, Graef IA, Crabtree GR (2007) NFAT signaling and the invention of vertebrates. *Trends Cell Biol* 17:251–260.
27. Tang CM, Insel PA (2004) GPCR expression in the heart; "new" receptors in myocytes and fibroblasts. *Trends Cardiovasc Med* 14:94–99.
28. Cowling RT, Gurantz D, Peng J, Dillmann WH, Greenberg BH (2002) Transcription factor NF-κ B is necessary for up-regulation of type 1 angiotensin II receptor mRNA in rat cardiac fibroblasts treated with tumor necrosis factor-α or interleukin-1 β. *J Biol Chem* 277:5719–5724.
29. Nishida M, et al. (2010) *Pertussis* toxin up-regulates angiotensin type 1 receptors through Toll-like receptor 4-mediated Rac activation. *J Biol Chem* 285:15268–15277.
30. Taylor BS, et al. (1998) Multiple NF-kappaB enhancer elements regulate cytokine induction of the human inducible nitric oxide synthase gene. *J Biol Chem* 273: 15148–15156.
31. Obasanjo-Blackshire K, et al. (2006) Calcineurin regulates NFAT-dependent iNOS expression and protection of cardiomyocytes: Co-operation with Src tyrosine kinase. *Cardiovasc Res* 71:672–683.
32. Ghosh S, Hayden MS (2008) New regulators of NF-kappaB in inflammation. *Nat Rev Immunol* 8:837–848.
33. Kelleher ZT, Matsumoto A, Stamler JS, Marshall HE (2007) NOS2 regulation of NF-kappaB by S-nitrosylation of p65. *J Biol Chem* 282:30667–30672.
34. Marshall HE, Stamler JS (2001) Inhibition of NF-κ B by S-nitrosylation. *Biochemistry* 40: 1688–1693.
35. Buss H, et al. (2004) Phosphorylation of serine 468 by GSK-3β negatively regulates basal p65 NF-kappaB activity. *J Biol Chem* 279:49571–49574.
36. Knowles RG, Moncada S (1994) Nitric oxide synthases in mammals. *Biochem J* 298: 249–258.
37. Gao H, et al. (2004) Identification of β-arrestin2 as a G protein-coupled receptor-stimulated regulator of NF-kappaB pathways. *Mol Cell* 14:303–317.
38. Witherow DS, Garrison TR, Miller WE, Lefkowitz RJ (2004) β-Arrestin inhibits NF-kappaB activity by means of its interaction with the NF-kappaB inhibitor IkappaBalpha. *Proc Natl Acad Sci USA* 101:8603–8607.
39. Kuhr FK, Zhang Y, Brovkovych V, Skidgel RA (2010) β-arrestin 2 is required for B1 receptor-dependent post-translational activation of inducible nitric oxide synthase. *FASEB J* 24:2475–2483.
40. Elton TS, Martin MM (2007) Angiotensin II type 1 receptor gene regulation: Transcriptional and posttranscriptional mechanisms. *Hypertension* 49:953–961.
41. Idzko M, et al. (2007) Extracellular ATP triggers and maintains asthmatic airway inflammation by activating dendritic cells. *Nat Med* 13:913–919.
42. Braun OO, Lu D, Aroonsakool N, Insel PA (2010) Uridine triphosphate (UTP) induces profibrotic responses in cardiac fibroblasts by activation of P2Y2 receptors. *J Mol Cell Cardiol* 49:362–369.

# EUにおける細胞・組織加工製品の規制動向

佐藤 陽治[*1, #], 鈴木 和博[*1], 早川 堯夫[*2]

医薬品医療機器レギュラトリーサイエンス
Vol. 42, No. 2 別刷（2011年）
財団法人 日本公定書協会

投稿/総説

医薬品医療機器レギュラトリーサイエンス
Pharmaceutical and Medical Device Regulatory Science
Vol. 42, No. 2, 142～148 (2011)

# EUにおける細胞・組織加工製品の規制動向

佐藤 陽治[*1,#]，鈴木 和博[*1]，早川 堯夫[*2]

（受付：平成22年10月29日，受理：平成22年12月27日）

# Regulation of Cell/Tissue-Based Medicinal Products in the European Union

Yoji SATO[*1,#], Kazuhiro SUZUKI[*1] and Takao HAYAKAWA[*2]

## はじめに

バイオテクノロジーや幹細胞学等の進展に伴い，再生医療・細胞治療などの先端医療で使用することを目的として，培養・活性化等の加工が施された生細胞を含む医薬品・医療機器（細胞・組織加工製品）が国内外で数多く開発されつつあり，今まで治療が困難であった疾患や重度の損傷への高い効果が期待されている．これらの開発の勢いに呼応し，細胞・組織加工製品の品質及び安全性を確保するための行政施策・規制をいち早く整備することは，細胞・組織加工製品の実用化を促進して患者のもとにいち早く届けるという意味の上からも，製品の国際競争力確保の意味の上からも大きな課題である．また，製品の効率的な国際流通を視野に入れた場合，世界各国・各地域における承認審査での有効性・安全性・品質評価に関する考え方についての理解及び国際的協調が不可欠である．

欧州連合（EU）では，細胞・組織加工製品は体細胞治療薬（somatic cellular therapy products）又は組織工学製品（tissue engineered products）の範疇に分類されている．従来，体細胞治療薬は遺伝子治療薬とともに先端医療医薬品（ATMP, advanced therapy medicinal products）という医薬品の一類型に分類されていたが，2008年12月より組織工学製品もATMPとして規制を受けることになった．また，同時にATMPの審査に特化した先端医療委員会(CAT)が創設されるなど，積極的な開発支援策が取られている．本稿ではEUにおける，これらの新しい取り組みについて概説する．

## 1. ATMPの規制の枠組み

EUでは，ATMPは欧州医薬品庁（EMA, European Medicines Agency）が販売承認審査を担当する．2008年12月以前はATMPの範疇に含まれる製品は，遺伝子治療薬（gene therapy products）と体細胞治療薬のみで組織工学製品が含まれておらず[1,2]，また，これらの製品の販売承認審査における評価基準に関して，EU加盟国間で統一がとれていなかった点が問題とされてきた．なおEUでは，医療機器に関しては，いずれかの加盟国より認定された民間の第三者認証機関の認証を受ければEU内の国境を越えた流通が可能となっており，国による審査は行われていないが，組織工学製品については医薬品[1]に分類されるか，医療機器[3,4]に分類されるか，その判断は加盟国によりまちまちであった．

欧州委員会（EC）はこれらの問題を，EU内で国境を越えた製品の流通を展開する際の大きな障壁であると考え，その解決策として2007年，ATMPの販売承認規制を定めるRegulation (EC) No 1394/2007[5]を定めた．Regulation (EC) No 1394/2007は，組織工学製品をATMPの範疇に加えること，及びATMPについては加盟国にお

*1 国立医薬品食品衛生研究所遺伝子細胞医薬部　東京都世田谷区上用賀1-18-1（〒158-8501）
Division of Cellular and Gene Therapy Products, National Institute of Health Sciences, 1-18-1 Kami-yoga, Setagaya, Tokyo 158-8501, Japan
*2 近畿大学薬学総合研究所　大阪府東大阪市小若江3-4-1（〒577-8502）
Pharmaceutical Research and Technology Institute, Kinki University, 3-4-1 Kowakae, Higashi-Osaka, Osaka 577-8502, Japan
# 責任著者 Corresponding author

ける承認審査を経ずに初めからEMAで中央審査を行うことなどを主な柱とし，2008年12月より施行されるに至っている．

## 2. Regulation（EC）No 1394/2007の概要

### 2.1 ATMPの定義

ATMPは，遺伝子治療薬，体細胞治療薬，又は組織工学製品と定義される．ここでの「体細胞治療薬」の定義は，「生物学的医薬品（biological medicinal product）のうち，(a) 意図する臨床上の用途に適うように生物学的性質，生理学的機能又は構造上の特性を変化させる実質的加工（substantial manipulation）を施された細胞・組織を含む製品又はこれらから成る製品，ないしはドナーの体内での本来の機能と同じ機能を患者の体内でも果たすことを意図して利用するのではない細胞・組織を含む製品又はこれらから成る製品で，(b) 製品に含まれる細胞・組織の薬理学的，免疫学的又は代謝的作用を通じて疾患の治療，予防又は診断を行うという観点に適う特性を有するもの，あるいはその観点からヒトに適用ないし投与されるもの」とされている[6]．一方，「組織工学製品」は「工学処理された細胞・組織を含む製品又はこれらから成る製品で，ヒト組織の再生，修復又は置換を行うという観点に適う特性を有するもの，あるいはその観点からヒトに適用ないし投与されるもの」を指す[5]．ここでの，「工学処理された細胞・組織」とは，「意図する再生，修復又は置換に適うように生物学的性質，生理学的機能又は構造上の特性を変化させる実質的加工を施された細胞・組織，ないしはドナーの体内での本来の機能と同じ機能を患者の体内でも果たすことを意図して利用するのではない細胞・組織」を指す（Table 1）．なお，「実質的加工ではない加工」の例としては，切断，研磨，成形，遠心分離，抗生剤・抗菌剤溶液への浸漬，殺菌・消毒・滅菌，放射線照射，細胞の分離・濃縮・精製，濾過，凍結乾燥，凍結，冷凍保存，ガラス化が挙げられている（文献5のAnnex I参照）．

従来，ある特定の組織工学製品が医薬品に該当するのか，医療機器に該当するのかという判断にEU加盟国間で差が生じやすかったことの大きな原因は，製品分類における「主要作用様式の原則」（primary mode of action rule）にあった．そこでRegulation (EC) No 1394/2007では，たとえ医療機器としての側面が主要作用様式であったとしても，組織工学製品の場合には，生きた細胞・組織を含むか否かという条件を優先し，医薬品の一種であるATMPに分類することとなっている．

### 2.2 ATMPに対する規制

#### 2.2.1 基本原則：リスクベースアプローチ

EUではATMPの販売承認に関する規制の原則として，リスクベースアプローチ（risk-based approach）が採られている（文献6のAnnex I Part IV参照）．リスクベースアプローチとは，審査対象となる各製品の性質に固有，かつその品質・安全性・有効性に関連するリスクの分析をベースにし，その影響の度合いを科学的に評価することにより規制の方針・内容を定めるという方法である．リスクベースアプローチは，日米欧医薬品規制調和会議（ICH）で2005年に合意された品質リスクマネージメント・ガイダンス（Q9）でも採用されており，今日では医薬品規制・開発の原則として比較的一般的なものとなっている．ATMPのリスクは，細胞の生物学的特性と由来，製造工程，ベクターの生物学的特性，タンパク質発現の様式，非細胞成分及び臨床におけるATMPの具体的な使用方法に大きく左右される．細胞を利用した製品については，その多様性の高さゆえに，患者，医療従事者又は公衆衛生に対するリスクの度合いも製品ごとに非常に異なってくる．したがって，こうした製品の開発計画及び審査要件は，多様な因子を加味したリスクベースアプローチによってケースバイケースで調節する必要があるとEMAは考えている[7]．同時にEMAは，ATMPの製造工程（製造工程内での検査や最終製品の検査を含む）は当該ATMPのリスクを十分に制限・制御できる能力を備えているべきだと考えており，また，非臨床試

**Table 1** EUにおける「体細胞治療薬」と「組織工学製品」の定義

| | 体細胞治療薬 | 組織工学製品 |
|---|---|---|
| 1. 使用目的 | 製品に含まれる細胞・組織の薬理学的，免疫学的又は代謝的作用を通じた疾患の治療，予防又は診断 | ヒト組織の再生，修復又は置換 |
| 2. 以下のいずれかに該当する細胞・組織を含む（又はそうした細胞・組織で構成される） | | |
| ・実質的加工* | 使用目的に適うように生物学的性質，生理学的機能又は構造上の特性を変化させる実質的加工を施された細胞・組織 | |
| ・細胞・組織の機能 | ドナーの体内での本来の機能と同じ機能を患者の体内でも果たすことを意図して利用するのではない細胞・組織 | |

* 実質的加工に含まれない加工の具体例については文献5のAnnex I参照

験及び臨床試験でも，同定されたリスク要因について深く検討すべきだとしている[8]．
（なお著者は，ここでいうリスクとは，所期の目標に対する「不適切性」，「不都合性」，「不合理性」，「非効率性」，「不確実性」などを意味していると解釈している．各ATMPの開発，製造，試験，審査，使用などの各過程や局面において，大小あるいは上位下位のさまざまな目標があり，アプローチがあるが，すべてが患者のためにという最終目的につながっているとの本質を常に認識・理解した上で，リスクアセスメント，コミュニケーション，コントロール，レビューなどを実施していくことが肝要である）．

#### 2.2.2 製品の品質・安全性・有効性に関する規制

ATMPは医薬品の一類型であり，従来の医薬品に関する様々な規制が適用される．つまり，市場で流通させるためには販売承認が必要であり，そのためには製品の品質・安全性・有効性を明示することと同時に，市販後の監視・調査が要求される．ATMPの製造に用いる細胞の提供・採取・検査はEUのGood Tissue Practice (GTP)[9~11]に従う必要があり，品質管理に関しては，EUのGood Manufacturing Practice (GMP)[12]に従う必要がある．なお，現在EMAはATMP向けの新しいGMPについても検討中である[13]．更に，ATMPと医療機器との複合製品の場合には，医療機器関連規制[3,4]に従うとともに，承認申請時には製品の物理的特性，機能様式及び設計方法に関して明らかにする必要がある．また，製品の特性概要・ラベリング・パッケージングの記載に関してはDirective 2001/83/EC[1]の要件に従うが，ATMPでは特に，ドナーの匿名性を尊重しつつも，細胞ないし組織の由来について，患者の知る権利に十分に即するようなものとなっている必要がある．

従来の医薬品・医療機器とは異なり多くのATMPは患者の体の一部となる．したがって，ATMPの有効性・副作用に関するフォローアップ及びリスクマネージメントをECは非常に重要視しており，申請者にはフォローアップ，市販後調査の詳細についての説明，またリスクマネージメント計画が求められる．ATMPの市販後フォローアップ及びリスクマネージメントに関してはEMAから詳細な指針が出されている[14]．また，ATMPの承認を受けた者は，その製品を使用する医療施設とともに，血液細胞以外の細胞・組織に関する規制[9]ないし血液細胞に関する規制[15]，及び個人情報保護に関する規制[16]に従い，患者・製品及び原材料のトレーサビリティを確保するシステムを構築・運用しなければならない．ATMPのトレーサビリティに関する詳細な指針については，現在検討中である．

## 3. ATMPの臨床試験

EUにおけるATMPの臨床試験は，日本における「治験vs.臨床研究」に相当する区分は存在せず，大学等における非商業目的の臨床研究に相当する試験であっても，すべて日本の治験に相当する規制が適用される．臨床試験（治験）後にEU域内で流通させる場合にはEMAによる中央審査が必要となる．ただし，EMAはあくまでも薬事承認審査を行う機関であり，治験の開始・実施に関する手続きはすべて加盟国の管轄となっている．すなわち，EMAは臨床試験には一切関与できない．

臨床試験に関しては，ICHの基準に従ったEUのGood Clinical Practice (GCP)[17]を順守することが必要であるが，Regulation (EC) No 1394/2007施行後のATMPの臨床試験に関しては，これに加え，現在策定中のATMP向けGCPに従う必要があるとされる．その詳細についてはトレーサビリティの確保等に関する留意点等がドラフト版[18]から垣間見ることができる．

治験に関する裁量がEU加盟各国に属することから，同一の治験届を各国に提出しても結論が国によって異なる恐れがある．逆に，加盟各国の規制や倫理基準に対応できるよう，治験届の内容に国別の修正を余儀なくされる可能性がある．こうした状況は，治験の科学的な価値を下げることになると危惧される．また，すべてのEU加盟国において治験参加者は等しく保護されるべきであるのが前提であることから，各国民の理解も得られにくくなってしまう．治験に関するハーモナイゼーションについてはEMAではなく，Heads of Medicines Agency (HMA)の臨床試験推進グループで議論されており，ガイダンス[19]を示す等の活動がなされている．

## 4. 相談制度・販売承認審査

### 4.1 相談制度

EMAは科学助言ワーキングパーティー（SAWP, Scientific Advice Working Party）を通じて医薬品の製品開発に関する科学的助言やプロトコール支援を開発者に提供している．ATMPの開発者は中小のベンチャー企業等（SME, Small and Medium-sized Enterprise）が多いことから，現在EMAでは，SMEがATMPについての科学的助言を必要とする場合，通常の手数料の90%割引で相談に応じている．相談者がSMEで，対象となるATMPが公衆衛生上の特別な利益となることが証明できる場合には，更なる割引が考慮される．なお，それ以外の開発者でも対象品目がATMPならば通常の65%割引で相談に応じている．また，オーファン医薬品の場

合のプロトコール支援は無料である.

ATMPに関する場合には，SAWPを通じた相談以外に，より非公式な制度として技術革新タスクフォース(ITF, Innovation Task Force) との相談も利用可能である．ITFはEMA内の多部局から成るグループで，法律・ガイドライン等が未整備な先端的治療・技術に関して規制面での問題点を議論することを目的としている．したがって，既存のガイドラインではカバーしきれないケースの多いATMPのような新規の製品については，開発者から規制面での疑問点をITFに投げかけることができる．この制度はITFから助言を受けるというよりもむしろ意見交換の意味合いが強い．ITFとの相談は無料であるが論議内容の法的拘束力はない.

更にこれらの制度とは別に，EMAの先端医療委員会(CAT, Committee for Advanced Therapies) は，開発者の品目がATMPに該当するか否かの助言を無料で行うとともに，SMEの非臨床試験・品質試験のデータの科学性に関する暫定認証を無料で行っている（後述).

### 4.2 ATMPの中央審査

EU内の国境を越えたATMPの流通に関しては，EMAがECからの委任を受けて一括して承認審査を行っており，そこで品質・安全性・有効性に関する科学的評価が行われている．EMA内でヒト向けの医薬品の販売承認審査を行うのは，ヒト用医薬品委員会 (CHMP; Committee for Human Medicinal Products) であるが，ATMPについては従来の医薬品・医療機器よりも専門的かつ多分野にわたる評価を要することから，CHMPの下部諮問組織として先端医療委員会 (CAT) が2008年12月末に設置され，CATでの品質・有効性・安全性の評価意見書案をもとにしてCHMPが承認審査を行い，CHMPが作成した評価意見書をもとにしてECが承認の判断をする，という体制が取られている．ATMPの品質・安全性・有効性確保に関する要件・評価をEU内で調和させ，直接的で迅速な流通を図る目的から，ATMPはEU加盟国内での審査を経ることなく，直接CATでの評価を受けることになった.

### 4.3 経過措置

2008年12月30日以前にEU内で流通が承認されたATMPに関しては，経過措置が取られる．組織工学製品ではないATMPの場合には3年の移行期間（2008年12月31日～2011年12月30日)，組織工学製品である場合には，4年の移行期間（2008年12月31日～2012年12月30日）が与えられており，それまでにATMPとしての再承認を受ける必要がある．期間内に再承認を受けない場合には，EU市場での承認は取り消される.

### 4.4 先端医療委員会（CAT）の構成と任務

#### 4.4.1 構成

先端医療委員会 (CAT) は，EU加盟国から各1名（副委員各1名)，患者団体から2名（副委員2名)，臨床医が2名（副委員2名）の，正副合計66名で構成され，会議は毎月1回開催される．患者団体及び臨床医の代表者としての委員はECが選定する．現在は，患者団体としてEGAN（欧州遺伝病連帯ネットワークEuropean Genetic Alliances' Network）及びEurordi（欧州希少疾病機構European Organisation for Rare Diseases)，臨床医の代表者としてESGCT（欧州遺伝子細胞治療学会European Society of Gene and Cell Therapy）及びEBMT（欧州血液骨髄移植グループEuropean Group for Blood and Marrow Transplantation）のメンバーがCATに参加している．なお，CHMPとの連携の必要性から，加盟国代表の委員うち5名はCHMPの委員である必要がある.

ATMPの評価において必要な学問領域としては，医療機器・組織工学・遺伝子治療・細胞治療・バイオテクノロジー・外科学・ファーマコビジランス・リスクマネージメント及び倫理学が挙げられており，委員会全体で必要な領域がカバーできるようにアレンジされている．その内訳は，遺伝子治療専門家が19%，細胞治療専門家が21%，組織工学の専門家が17%，バイオテクノロジー専門家が24%，倫理学専門家が8%，ファーマコビジランス専門家が5%，医療機器専門家5%，外科学専門家1%となっている.

#### 4.4.2 CATの任務

CATの任務には，①ATMPの科学的評価，②ATMP該当性に関する助言，③SMEのATMP品質・非臨床データの暫定認証，④SAWPへの協力，そのほか，ATMP以外の製品についてのCHMPとの相談，及びECへの助言などがある.

4.4.2.1 ATMPの科学的評価

CATの任務の中でも主要なのは，ATMPの科学的評価である．個別のATMPについて，CATは品質・安全性・有効性に関する科学的評価結果を意見書案としてCHMPに提出する．評価意見書案の提出は，正式な承認申請日から数えて約200作業日以内に行う．なお，CHMPは正式な承認申請日から数えて210作業日以内に承認に関する評価意見書を確定する．なお，これら作業日には土日祝日を含む．また，CATの質問事項リストが出された時から申請者がこれに回答するまでの間は作業日に勘定しない．ATMPが医療機器との複合製品

の場合には，CATは医療機器認証機関との情報交換も行う．

4.4.2.2　ATMP該当性に関する助言

CATは特定の品目がATMPに該当するか否かについて，科学的な基準に基づいた検討・判断を行う．製品の分類に関する助言要請は，治験届や承認申請の有無に係らず随時受け付けられており，手数料もかからない．正式な助言要請から60日以内で回答されることになっている．CATの回答は，製品の内容・治療対象・CATによる検討結果について，秘匿事項を除いた後に公開される．また，ATMPのファーマコビジランス及びリスクマネージメントシステムの計画及び実施に関しても，承認申請者・承認取得者からの要請に応じて助言を行う．

4.4.2.3　SMEのATMP品質・非臨床データの暫定認証

中小ベンチャー企業等（SME）はATMPの品質・非臨床データに関し，CATによる科学的評価に基づく暫定認証を受けることができる．暫定認証の審査は治験開始・承認申請の有無に係らず，SMEから申請があった場合に随時行われる．あくまで品質・非臨床データの科学的評価の結果のみを認証するものであって，治験届や承認申請とは独立したものとみなされている．すなわち，認証書は法的には治験届や承認申請の際に提出すべきデータの代用として使うことはできない．ただしECとしては，同じデータを用いて将来，治験あるいは承認の申請が行われる際には，申請の評価が行いやすくなることも期待している．

4.4.2.4　SAWPへの協力

CATはSAWPに協力することにより，ATMPの科学的助言にも関与している．ただし，CATのSAWPへの関わり方の詳細については試行錯誤が続いている．

### 4.5　ATMP承認審査におけるEMA各組織の役割

#### 4.5.1　CATとCHMPの共同作業

従来の医薬品の場合はCATに諮問されることなく，CHMPラポーターとCHMP副ラポーターがそれぞれ専門家チームを構成して評価し，その評価結果をCHMPで議論する．結論がCHMPで了承されると，それを受けたECが承認をすることになる．一方，ATMPの評価はCATラポーターとCHMPコーディネーター及び品質・安全性・有効性の各専門家からなるチームと，CAT副ラポーターとCHMP副コーディネーター及び品質・安全性・有効性の各専門家からなるチームの2チームで行う．2チームが作成した評価レポートをCHMPのメンバー1名とCATのメンバー1名以上が査読し，その結果をCATの全体会議で議論する．CATは議論した内容を評価意見書案としてCHMPに提出する．CHMPは評価意見書案をもとに承認審査を行って評価意見書を作成し，更にこれをもとにECが承認の可否を判断する．

#### 4.5.2　CATの役割

先述のようにCATはATMPの科学的評価を行うことになっているが，具体的作業としては，ATMPの評価に関して質問事項のリスト，解決すべき問題点のリスト，及び評価意見書案の内容を議論する．また，必要となれば会議中にEMAのワーキングパーティーメンバー等の外部専門家にもスライドと電話でのプレゼンテーションをさせ，議論を行う．CAT正副ラポーターは，CATの全体会議における評価の過程・議論をコーディネートするとともに，評価レポート，質問事項リスト，問題点リスト等の作成を担当し，またEMAのワーキングパーティーメンバー等の外部専門家との相談の必要性があるかどうかの判断を行う．

#### 4.5.3　CHMPの役割

CHMPはATMPの評価を行う2チームの任命を行うともに，CATの評価意見書案をもとにした評価意見書を作成する．また，CATでの評価過程でコメントを加えることもできる．全体会議で主なATMPについての科学的意見や議論について情報を共有し，必要であれば審査期間（正式な承認申請日から数えて210日作業日）の最後に問題点リストの作成及び口頭での説明の機会設定を行うことができる．

CHMP正副コーディネーターは，CATの上部組織であるCHMPとCATとの間の情報のパイプ役となるとともに，CHMPにおいてCATの意見についての討議・採択を担当する．また，審査期間中にEMAのワーキングパーティーメンバー等の外部専門家との相談の必要性があるかどうかの判断を行う．

#### 4.5.4　EMA事務局の役割

EMAはCATの評価意見書案及びCHMPの評価意見書がそれぞれ決められた期間内に作成されることをチェックすると同時に，CAT及びCHMPの評価の透明性を確保する．CAT事務局は，CAT正副ラポーターの評価レポートの科学的面及び規制の面での整合性を確保すると同時に，CHMPでの最終承認を受けるための評価意見書案の準備を行う．更に，CAT事務局はATMPの評価や回収に関する情報収集・提供を行う．

## 5.　市販後安全対策

Regulation（EC）No 1394/2007には，ATMP市販後における安全対策として，トレーサビリティの確保と市販後における安全性監視（ファーマコビジランス）が挙げられている．ATMPのドナー・原材料・製品・製造工程